Late Pleistocene structural evolution of the Camarillo fold belt: Implications for lateral fault growth and seismic hazard in Southern California

Duane E. DeVecchio[1], Edward A. Keller[2], Markus Fuchs[3], and Lewis A. Owen[4]
[1]EARTH RESEARCH INSTITUTE, UNIVERSITY OF CALIFORNIA, SANTA BARBARA, CALIFORNIA 93106-9630, USA
[2]DEPARTMENT OF EARTH SCIENCE, UNIVERSITY OF CALIFORNIA, SANTA BARBARA, CALIFORNIA 93106-9630, USA
[3]DEPARTMENT OF GEOGRAPHY, JUSTUS-LIEBIG-UNIVERSITY GIESSEN, D-35390 GIESSEN, GERMANY
[4]DEPARTMENT OF GEOLOGY, UNIVERSITY OF CINCINNATI, CINCINNATI, OHIO 45221, USA

ABSTRACT

The Camarillo fold belt in the Western Transverse Ranges poses a significant seismic hazard to nearly one million people living in Southern California, yet few published geologic or geochronological data from this fold belt exist. The Camarillo fold belt is composed of several south-verging, west-plunging anticlines that characterize the western extent of the Simi fault zone, which extends for 40 km through urbanized Ventura and Los Angeles Counties. Surface and subsurface geologic data are utilized to accurately construct five cross sections within discrete structural domains to assess the local style of deformation, and to quantify the magnitudes of fault slip, fault- and fold-related uplift, and percent shortening. Eight new optically stimulated luminescence (OSL) dates from three paleoseismic trenches and six numerical dates from a previous study were utilized to quantify the timing and rates of deformation on discrete faults and folds. The onset of deformation in the Camarillo fold belt is everywhere younger than ca. 125 ka and locally as young as ca. 25 ka. Quaternary deformation occurs on reactivated steeply dipping (70°) Miocene faults, with shortening being largely accommodated in a narrow zone (<2 km) of folding where fold-related uplift is typically twice as great as hanging-wall uplift in response to fault slip. A minimum fault slip rate between 0.8 mm/yr and 1.4 mm/yr, a recurrence interval of 715–1100 yr, and a maximum M_w 6.8 earthquake for faults within the Simi fault zone is estimated, which are comparable to other better-studied fold belts in Southern California. A model of punctuated lateral fault propagation is proposed to explain westward growth of the Simi fault, which occurs in discrete pulses that are separated by intervals of fault displacement accumulation and fold amplification during constant-fault-length conditions. Lateral fault growth is limited in space and time by an orthogonal north-striking fault set, which juxtaposes a series of west-plunging anticlines that decrease in structural relief and age toward the west.

LITHOSPHERE; v. 4; no. 2; p. 91–109. doi: 10.1130/L136.1

INTRODUCTION

The Working Group on California Earthquake Probabilities (WGCEP, 1995, 2007) identified a continuous belt of deformation south of the San Andreas fault between Los Angeles and Ventura that has the potential to produce more than four damaging earthquakes in the next century (Fig. 1). Extremely high rates of contractional deformation across the region are suggested by continuous global positioning system measurements (7–15 mm/yr; Donnellan et al., 1993; Shen et al., 2003) and geologic studies (25 mm/yr; Huftile and Yeats, 1995). Shortening is accommodated on east-striking reverse faults, which in the past 30 yr of the twentieth century produced three destructive earthquakes (Fig. 1). Consequently, significant earthquake hazard research within active fold belts has successfully quantified the rates of late Quaternary deformation, and determined the recent history of faulting on numerous individual structures in Southern California (e.g., Rockwell et al., 1984; Yeats et al., 1988a; Larsen et al., 1993; Dolan et al., 2000, 2003; Oskin et al., 2000; Keller and Gurrola, 2000). However, the Camarillo fold belt, which lies between the Los Angeles–Santa Monica and Ventura fold belts (Fig. 1), has not yet been studied in detail for the purpose of quantifying the precise timing, rates, and magnitudes of contractional deformation. Therefore, this region represents a significant gap in the quantification of the distribution of strain in space and time across this part of the plate boundary. In addition, understanding and defining the nature and dynamics of active fold belts and lateral fault growth are areas of considerable interest in active tectonics (e.g., Jackson et al., 1996; Childs et al., 2003; Ramsey et al., 2008; Keller and DeVecchio, 2012). Therefore, this region has the potential to be an analog for future studies of young active fold belts.

The Camarillo fold belt, located in the Western Transverse Ranges, is composed of several active south-verging fault-related folds that constitute the highly segmented western extent of the Simi fault zone (Fig. 2). These faults pose a significant hazard to nearly one million people living in the cities of Ventura, Camarillo, Thousand Oaks, and Oxnard, as well as those living in the Simi and Santa Clara River Valleys (Fig. 2). Descriptions of unlithified, but folded and faulted fluvial sands and silts in the Camarillo fold belt are common in consulting reports and paleoseismic trench logs and are commonly ascribed to the Saugus Formation (e.g., Earth Systems Southern California, 2005; Boales, 1991; Gonzalez and Rockwell, 1991; Geosoils Inc., 2006). Based on magnetostratigraphy and amino acid racemization on shells from an overlying marine terrace, the Saugus Formation has an estimated age range of ca. 2500 ka to ca. 500–200 ka (Lajoie et al., 1982; Yerkes, et al., 1987; Levi and Yeats, 1993). However, DeVecchio et al. (2012) showed that the Saugus Formation in the Camarillo fold belt is compositionally different and locally unconformable with Saugus strata north of the study area. In addition, these strata are considerably

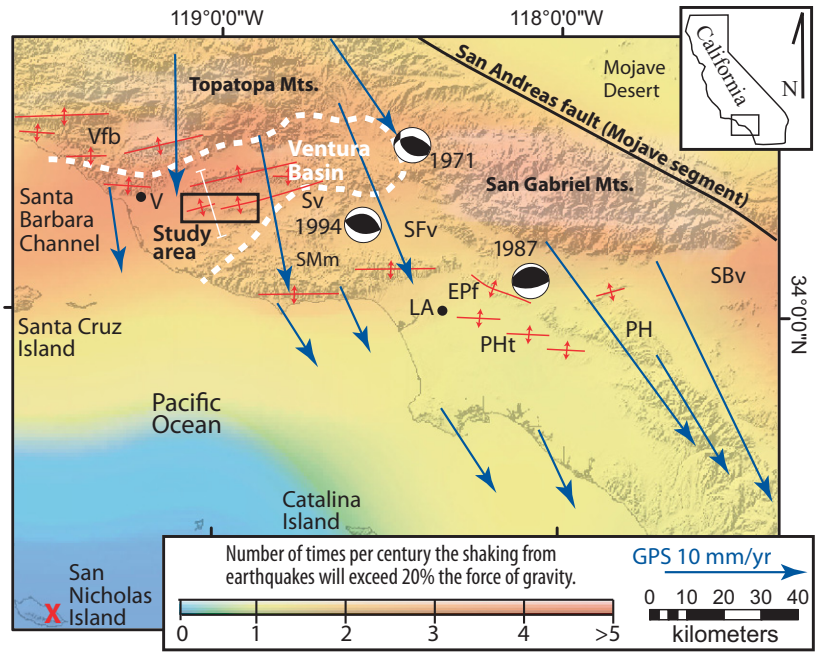

Figure 1. Regional index map of Southern California showing the topography, geographic localities, potential future occurrence of damaging earthquakes (color shading), global positioning system (GPS) velocities (blue arrows), studied fold belts (red lines), previous cross section (white line, location of Fig. 3), and selected compressional earthquake events with respect to the study area (black box). Color shading (modified from WGCEP, 1994) indicates that the Ventura Basin (outlined in dashed white line) is likely to experience more than four damaging earthquakes in the next century. Selected GPS vectors from Shen et al. (2003) illustrate the north-south contractional strain across the Western Transverse Ranges modeled for nonlocked faults, but corrected for the effects of large earthquakes. Lower-hemisphere earthquake focal mechanisms, labeled by year, are from the scientists of the U.S. Geological Survey and Southern California Earthquake Center (1994), and they show the approximate epicentral locations of three destructive compressional earthquakes: 1971 M_w 6.6 San Fernando/Sylmar; 1987, M_w 6.0 Whittier Narrows; and 1994 M_w 6.7 Northridge. Geographic localities discussed in the text include: EPf—Elysian Park fault; LA—Los Angeles; PH—Puente Hills; PHt— Puente Hills thrust; SFv—San Fernando Valley; SMm—Santa Monica Mountains; Sv—Simi Valley; SBv—San Bernardino valley; V—City of Ventura; Vfb—Ventura fold belt.

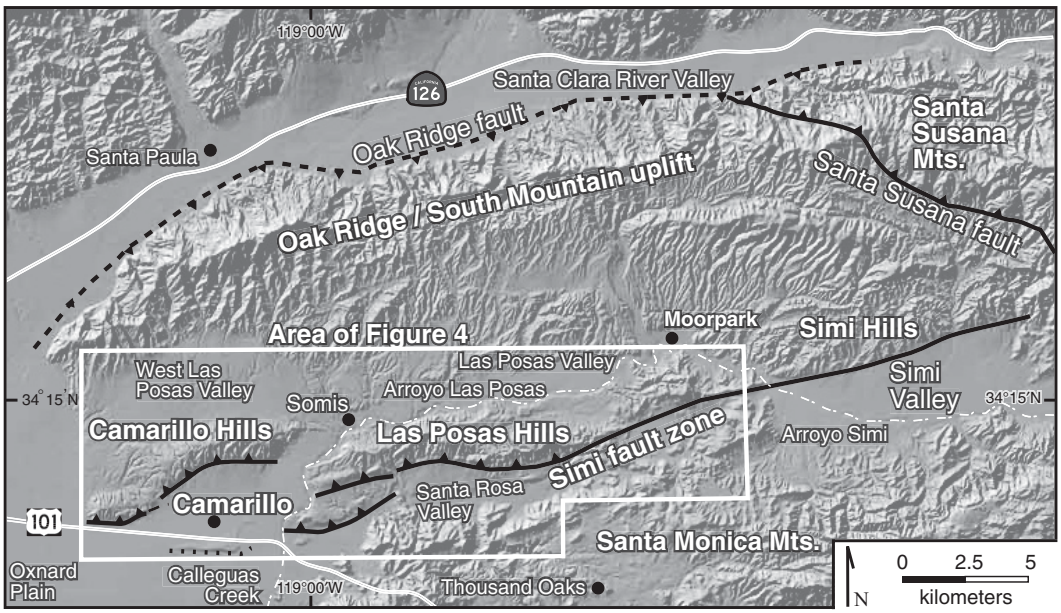

Figure 2. Shaded relief map showing the local topography and geologic and geographic features with respect to the Camarillo fold belt (white box). Note that the Camarillo fold belt constitutes the western extent of the Simi fault zone, which delineates the northern boundary of the Simi Valley and uplifts the Simi Hills east of the study area.

younger than Saugus strata elsewhere, having a lower maximum age of ca. 125 ka and an inferred upper age of ca. 75 ka (DeVecchio et al., 2012); this has significant implications for fault slip-rate estimates from previous studies, as well as in this study.

This paper examines the late Quaternary structural development and geomorphic evolution of the Camarillo fold belt. Surface and subsurface analysis and eight new optically stimulated luminescence (OSL) ages from a paleoseismic trench are presented and integrated with geochronologic results of DeVecchio et al. (2012) from deformed Saugus strata and offset strath terraces to quantify the magnitudes and rates of deformation. These data indicate that the Camarillo fold belt is characterized by rapid structural development, with the initiation of all faulting in the study area beginning after 125 ka and locally after 25 ka. Deformation is controlled by two inherited Miocene fault sets, which result in punctuated lateral propagation of the Simi fault toward the west. Long-term late Pleistocene fault slip rates are greater than previous estimates based on paleoseismic investigations and are similar to other better-studied fold belts in the region (e.g., Dolan et al., 2000; Oskin et al., 2000). In addition, these results provide new insights into the structural evolution and processes that control lateral fault growth in nascent fault zones in Southern California.

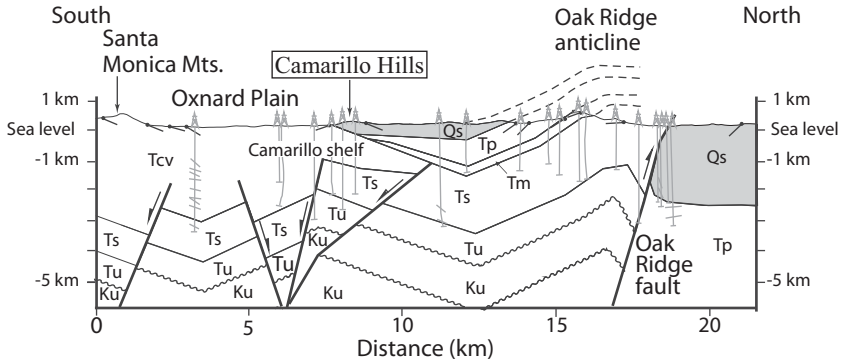

Figure 3. Balanced cross section showing the relationship of deep subsurface structure of the Oak Ridge fault hanging wall with respect to the Camarillo fold belt (modified from Namson and Davis, 1991). See text for discussion of the Camarillo shelf. The location of the cross-section line is shown on Figure 1. Tcv—Conejo Volcanic; Ku—Cretaceous undifferentiated; Qs—Saugus Formation; Tm—Monterey/Modelo Formation; Tp—Pico Formation/Fernando Group; Ts—Sespe Formation; Tu—Tertiary undifferentiated.

GEOLOGIC SETTING

Regional Structural and Stratigraphic Framework

The California borderlands, west of the San Andreas fault, have experienced a polygenetic tectonic evolution following cessation of subduction during early Miocene time, including microplate capture, clockwise rotation in excess of 90°, and syntectonic volcanism (e.g., Kamerling and Luyendyk, 1979; Luyendyk et al., 1980; Nicholson et al., 1994; Weigand et al., 2002), as well as transpressional deformation related to the "Big Bend" of the San Andreas fault (e.g., Wright, 1991; Dolan et al., 1995; Shaw and Suppe, 1996; Yeats, 1988a). Thick sections of volcanic and volcaniclastic rocks of the Conejo volcanics and deep-marine siliceous mudstones (Monterey Formation) accumulated in middle Miocene fault-bounded transtensional basins, with the Oligocene Sespe Formation on the upthrown fault block (Fig. 3; Kew, 1924; Durrell, 1954; Ehrenspeck, 1972; Jakes, 1979; Namson and Davis, 1988; Williams, 1983; Ingersoll, 2001). Extensional deformation continued until ca. 5 Ma, at which time development of the "Big Bend" of the San Andreas fault resulted in transpressional deformation and inversion of Miocene basins (e.g., Crowell, 1976; Wright, 1991). The modern structure and Quaternary shortening of the region are strongly influenced by the transrotational history as indicated by reactivation of Miocene faults as east-striking high-angle reverse faults (Jakes, 1979; Hanson, 1980; Yeats, 1988b; this study).

Following Miocene transtension and volcanism, deep-marine basins were filled by a progradational sequence of Pliocene–Pleistocene deep-marine turbidites, shallow-marine sandstone and mudstone, and terrestrial sandstone and conglomerate (Kew, 1924; Winterer and Durham, 1958; Weber et al., 1976; Yeats, 1965, 1977; Dibblee, 1992a). During the early Pleistocene, the Camarillo fold belt was situated on what Yeats (1965) referred to as the Camarillo shelf, where most of the late Tertiary sediments (i.e., Monterey Formation [Tm] and Pico Formation [Tp]; Fig. 3) were not deposited or had been erosionally removed during the middle to late Pleistocene (Yeats, 1965; DeVecchio et al., 2012).

Within the Camarillo fold belt, a thin section (40–60 m) of terrestrial strata conformably overlies fossiliferous shallow-marine sediments (e.g., Jakes, 1979; Dibblee, 1992a; DeVecchio et al., 2012). Although many names have been applied to these strata (see fig. 3 of DeVecchio et al., 2012), we follow the nomenclature of Pressler (1929) and Dibblee (1990, 1992a) and apply the name Las Posas Sand to the underlying shallow-marine strata and Saugus Formation to the terrestrial strata. However, DeVecchio et al. (2012) showed that the Las Posas Sand and Saugus Formation exposed in the Camarillo fold belt are significantly younger than these geologic units elsewhere in the Ventura Basin, with the entire Pleistocene section having been deposited after ca. 140 ka. The Saugus Formation in the Camarillo fold belt is diachronous, having a lower age limit that gets younger from east to west, from ca. 125 ka in the eastern part of the study area to ca. 80 ka in the west (Fig. 4A; DeVecchio et al., 2012). In addition, DeVecchio et al. (2012) correlated the Saugus strata in the Camarillo fold belt to sediments of the Mugu aquifer in the Las Posas and Santa Rosa Valleys (Fig. 2), which have the same provenance and thickness (Hanson et al., 2003), and overlap in age (Dahlen, 1992). Therefore, in order to avoid genetic and temporal confusion with Saugus strata elsewhere in the Ventura Basin, DeVecchio et al. (2012) applied the name "Camarillo Member" to Saugus strata (Qscm) deformed in the Camarillo fold belt (Fig. 4).

Local Physiography and Structure

The Simi fault delineates the northern boundary of the Simi Valley and extends for 40 km to the west into the Oxnard Plain near the city of Camarillo (Fig. 2). Within the study area, the Simi fault becomes a broad zone of deformation composed of several discrete fault segments and folds, which constitute the Camarillo fold belt. The Camarillo fold belt is situated in the topographic low between the Oak Ridge–South Mountain uplift and the Santa Monica Mountains (Fig. 2), in the hanging wall of the south-dipping Oak Ridge fault (Fig. 3).

Folded strata are exposed in the Camarillo Hills, north of Camarillo, and in the Las Posas Hills north of Santa Rosa Valley (Fig. 2). These hills are characterized by low-relief (<250 m), south-verging anticlinal folds developed in the Saugus Formation and the Las Posas Sand, which unconformably overlie Oligocene and Miocene bedrock (e.g., Yeats, 1965; Jakes,

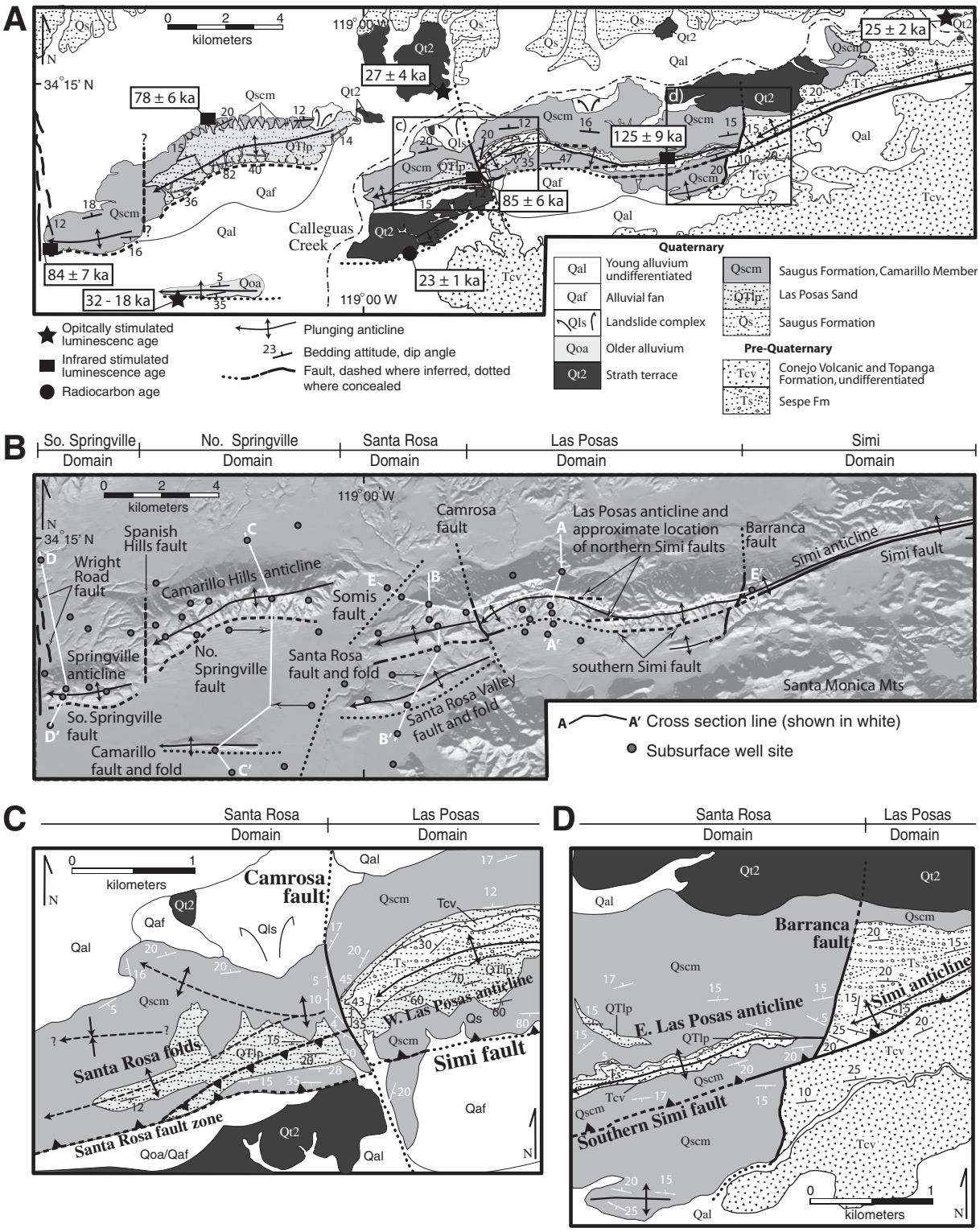

Figure 4. Maps of the Camarillo fold belt. (A) Geologic map of the Camarillo fold belt and a part of the Santa Monica Mountains (see Fig. 2 for location). Numerical dates are shown in white boxes, which are linked to one of three different symbols, which indicate the type of geochronological technique that was used to determine the age. (B) Structure map of the Camarillo fold belt draped over topography including the names of the different structures discussed in the text and approximate east-west extents of discrete structural domains. The boundaries between domains are delimited by the presence of north-striking cross faults, across which the style, timing, and magnitude of deformation change (i.e., Wright Road, Spanish Hills, Somis, Camrosa, and Barranca faults). North-south cross sections A through D are shown in Figure 6, and east-west cross section E-E′ is shown in Figure 8. Well sites show the location of petroleum and water wells of Jakes (1979) and Hanson et al. (2003) utilized in this study. Note that the northern Simi fault splays in the Los Posas domain are approximated by the location of the Las Posas anticlinal axis. (C–D) Close-up views of contrasting geology juxtaposed across the Camrosa and Barranca faults, respectively; the locations are shown in A.

1979, Dibblee, 1990, 1992a, 1992b). Folds are developed above north-dipping reverse faults that are locally exposed at the surface, but are commonly concealed beneath younger alluvium (Jakes, 1979; Blake, 1991a; Treiman, 1997, 1998). Anticline forelimbs on the south flanks of folds typically dip more steeply (35°–80°) and are more incised than the gently dipping back limbs (10°–25°; Fig. 4A). The Camarillo and Las Posas Hills are separated by a water gap created by Calleguas Creek, which drains the Arroyo Las Posas and Arroyo Simi (Fig. 2). An additional fault trend south of the city of Camarillo and west of Calleguas Creek (Camarillo fault of Jakes, 1979) deforms fluvial strata into a low-relief (<25 m), undissected anticline within the Oxnard Plain (Fig. 4B). Strata deformed in the Camarillo anticline are identified as the Saugus Formation in paleoseismic trenches (Earth Systems Southern California, 2005; Geosoils Inc., 2006) and as older alluvium by Jakes (1979).

Although no fault scarps are known in the Camarillo fold belt, several paleoseismic investigations have shown Holocene displacement along the Simi fault zone. A paleoseismic trench in the western Simi Valley documented 2–2.5 m of left-lateral oblique displacement on the Simi fault, with the last event occurring as recently as 1200 cal. yr B.P. (Hitchcock et al., 1998). Paleoseismic investigations by Gonzalez and Rockwell (1991) across the southern Springville fault (Fig. 4B) indicated a displacement of 0.65–1.1 m per seismic event, a recurrence interval of 720–2200 yr, and a slip rate of 0.5–0.9 mm/yr based on two fault offsets and the inferred ages of several colluvial deposits.

METHODS OF INVESTIGATION

Surface and Subsurface Mapping

Our mapping builds upon previous regional-scale mapping (Kew, 1924; Bailey, 1951), unpublished thesis maps (Pasta, 1958; Jakes, 1979; Hanson, 1980), 1:24,000 scale quadrangle maps (Dibblee, 1990, 1992a, 1992b), and professional reports (e.g., Treiman, 1997, 1998; Blake, 1991b). Although previous mapping adequately shows the distribution of geologic units and the surface traces of many of the faults, we field checked geologic contacts and collected structural data along all of the exposed fault zones as well as several previously unrecognized fault traces. In addition, we collected stratigraphic data and geochronological samples along the basal contact of the Saugus Formation with the underlying Las Posas Sand (Fig. 4A) in order to assess the nature and timing of the transition from shallow-marine to terrestrial deposition. The basal contact of the Camarillo Member of the Saugus Formation is exposed along most of the anticlinal cores and can be identified in subsurface well data; therefore, when precisely dated, this datum can be used as a strain marker from which to assess the timing and rates of deformation along the fold belt. In addition, we mapped and dated a late Pleistocene strath terrace level (Qt2), which is locally deformed by faulting. Where extensive recent urbanization conceals geologic contacts and structural data, such as the Springville anticline, we relied solely upon previous mapping.

Previous geologic maps were digitized and integrated into a geographic information system (GIS)–based system of observation and analysis. Utilizing a handheld computer running ESRI ArcPad with integrated global positioning system (GPS), we were able to accurately locate structural and lithologic contacts mapped by previous researchers, even where landforms had been modified by human development. Due to extensive agricultural use and urbanization of the Qt2 surface, terrace levels were correlated based on their degree of dissection, elevation continuity, and age. See DeVecchio et al. (2012) for discussion of the Qt1 strath terrace, which is mapped north of the study area on the south flank of the Oak Ridge–South Mountain uplift.

Geologic surface relations were compared to more than 50 subsurface wells, compiled by Jakes (1979), and Hanson et al. (2003) (Fig. 4B). Previous workers' lithologic interpretations of electronic logs and drill cores were relied upon to accurately locate subsurface structure and unit contacts, and to determine subsurface fault and bedding dips. Jakes (1979) did not differentiate between Pleistocene terrestrial strata and marine strata in subsurface data. Therefore, we combined those data with a U.S. Geological Survey (USGS) Water Resources Investigation report (Hanson et al., 2003), which clearly describes the lithology and illustrates the subsurface aquifer system of the region in a series of cross sections, which traverse the Camarillo fold belt. We constructed cross sections to quantify the magnitudes of deformation on faults and folds by integrating surface and subsurface geologic constraints and correlating the Camarillo Member of the Saugus Formation strata with the Mugu aquifer of Hanson et al. (2003) (DeVecchio et al., 2012).

Geochronological Approaches and Technique

The focus of our geochronology investigation was to numerically date deformed geologic contacts and geomorphic surfaces to quantify deformation rates. This study includes eight new OSL quartz analyses, collected from three paleoseismic trenches across the Camarillo anticline (Fig. 4A). In addition, we include results from three infrared stimulated luminescence (IRSL) measurements on feldspar samples collected from the base of the Camarillo Member of the Saugus Formation and two quartz OSL analyses from sediments that overlie the Qt2 strath terrace from DeVecchio et al. (2012) (Table 1).

The luminescence signal derived from OSL and IRSL records the elapsed time since the sediment was last exposed to sunlight during the reworking process of erosion, transportation, and deposition and therefore, represents the burial age (e.g., Aitken, 1998). Samples were collected in light-safe tubes from sand bodies. Equivalent dose measurements (D_e) were determined on multiple aliquots for each sample using the single-aliquot regeneration-dose (SAR) protocol of Murray and Wintle (2000) (Fig. 5). A dose recovery test was applied to test for an appropriate preheat and cut-heat temperature. With a preheat temperature of 260 °C and a cut heat of 200 °C, we were able to reconstruct the given dose within a 5% error range. The recycling ratios of all measurements were within the 10% limits, and the recuperation was below 5%. On average, 10 aliquots (and in some cases, as many as 25) were measured from individual samples using the coarse-grained fraction (90–125 μm). Quartz mineral separates were prepared and analyzed at the University of Cincinnati, whereas feldspar preparation and analyses were conducted at the University Bayreuth, Germany. Radioisotope concentrations for sediment samples were determined using neutron activation analysis at the USGS Nuclear Reactor in Denver.

Both OSL and IRSL aliquots showed high D_e scatter (Fig. 5C). The scatter in D_e measurements suggests that all samples may have experienced insufficient bleaching (solar resetting), which may produce overestimates of the true age of the sediment (Murray et al., 1995; Aitken, 1998; Wallinga, 2002). Assuming insufficient bleaching of the grains during their last sediment reworking, we used a model to calculate the D_e from the lower part of the dose distribution, which represents the best-bleached grains (Murray et al., 1995; Fuchs and Lang, 2001; Wallinga, 2002; Fuchs and Wagner, 2003; Fuchs et al., 2007). The model uses the following approach: (1) D_e values for each sample are ordered from lowest to higher values (Fig. 5C). (2) Starting with the two lowest D_e values, arithmetic mean D_e values are calculated, with the number of values increasing by one in each step. (3) The procedure is repeated until a relative standard deviation threshold (derived from the artificially irradiated sample) is just exceeded. This mean value was then used for age calculation. Because water content affects

TABLE 1. ANALYTICAL RESULTS FROM OPTICALLY STIMULATED LUMINESCENCE (OSL) GEOCHRONOLOGY FROM THE CAMARILLO FOLD BELT

Sample number	Location*		Method	Unit	^{238}U (ppm)	^{232}Th (ppm)	^{40}K (%)	$\Delta W^{\dagger}$	Cosmogenic dose rate, DR_{Cosm} (Gy/k.y.)§	Total dose rate (Gy/k.y.)	D_e (Gy)#	Age (ka)**
	Easting	Northing										
1	323595	3791611	IRSL	Qscm	0.69 ± 0.07	2.46 ± 0.05	2.72 ± 0.05	1.15 ± 0.07	0.15 ± 0.01	3.07 ± 0.19	386.48 ± 11.6	125 ± 9††
2	306417	3789099	IRSL	Qscm	2.71 ± 0.03	7.82 ± 0.04	2.54 ± 0.23	1.15 ± 0.07	0.14 ± 0.01	3.79 ± 0.28	318.4 ± 10.8	84 ± 7††
3	310474	3792386	IRSL	Qscm	4.91 ± 0.05	10.81 ± 0.05	2.22 ± 0.20	1.15 ± 0.07	0.17 ± 0.01	4.19 ± 0.29	326.7 ± 7.0	78 ± 6††
4	318247	3791107	IRSL	Qscm	4.75 ± 0.05	7.32 ± 0.03	2.63 ± 0.16	1.15 ± 0.07	0.15 ± 0.01	4.27 ± 0.28	365.1 ± 10.3	85 ± 6††
5	332000	3795598	OSL	Qt2	2.71 ± 0.05	7.93 ± 0.05	2.39 ± 0.16	1.15 ± 0.07	0.17 ± 0.01	3.25 ± 0.25	80.23 ± 2.09	25 ± 2††
6	317585	3793613	OSL	Qt2	1.33 ± 0.03	4.13 ± 0.03	2.56 ± 0.19	1.15 ± 0.07	0.20 ± 0.01	2.87 ± 0.28	78.18 ± 9.99	27 ± 4††
7	310551	3787785	OSL	Qoa	1.48 ± 0.03	5.91 ± 0.05	2.77 ± 0.18	1.15 ± 0.07	0.15 ± 0.01	3.17 ± 0.25	81.94 ± 11.38	26 ± 4
8	310551	3787785	OSL	Qoa	1.40 ± 0.03	4.27 ± 0.03	2.99 ± 0.17	1.15 ± 0.07	0.15 ± 0.01	3.25 ± 0.25	65.26 ± 7.95	20 ± 3
9	310559	3787797	OSL	Qoa	1.41 ± 0.03	4.29 ± 0.03	2.63 ± 0.17	1.15 ± 0.07	0.17 ± 0.01	2.96 ± 0.23	95.59 ± 17.07	32 ± 6
10	310895	3787709	OSL	Qoa	2.06 ± 0.04	6.61 ± 0.05	2.81 ± 0.19	1.15 ± 0.07	0.14 ± 0.01	3.36 ± 0.26	93.32 ± 2.13	28 ± 2
11	310911	3787679	OSL	Qoa	2.21 ± 0.04	8.77 ± 0.07	2.22 ± 0.19	1.15 ± 0.07	0.11 ± 0.01	2.99 ± 0.24	54.62 ± 2.85	18 ± 2
12	310895	3787709	OSL	Qc1	2.10 ± 0.04	7.96 ± 0.06	2.43 ± 0.18	1.15 ± 0.07	0.14 ± 0.01	3.12 ± 0.25	91.04 ± 19.71	29 ± 8
13	310895	3787709	OSL	Qc1	2.13 ± 0.04	9.39 ± 0.08	2.34 ± 0.19	1.15 ± 0.07	0.14 ± 0.01	3.14 ± 0.25	93.32 ± 4.73	30 ± 3
14	310914	3787679	OSL	Qc2	2.18 ± 0.04	9.41 ± 0.07	2.10 ± 0.18	1.15 ± 0.07	0.14 ± 0.01	2.95 ± 0.24	120.06 ± 5.96	41 ± 4

*Locations are given in Universal Transverse Mercator (UTM) coordinates system zone 11, using World Geodetic System 1984 (WGS84) datum.
†Estimated water content given in the Δ notation (weight wet sample/weight dry sample) (Aitkin, 1985).
§Cosmic doses and attenuation with depth were calculated using the methods of Prescott and Stephan (1982) and Prescott and Hutton (1994).
#Average equivalent dose (D_e) and error ($1\sigma_{n-1}$ of the D_e), incorporating the error from beta source estimated at about ±5%.
**Errors for OSL and infrared stimulated luminescence (IRSL) uncertainties in the equivalent doses, dose rates, and age determinations are expressed at the 1σ confidence level.
††Numerical results from DeVecchio et al. (2012).
Note: See figure 4A for unit names.

the dose rate, and the water content since the time of burial is unknown, we assumed an error for the water content. This error represents a possible minimum and maximum water content, which is given by the pore volume and its pore-size distribution within the sediment. A good estimation of the pore volume and pore-size distribution can be made using the grain-size distribution (Scheffer and Schachtschabel, 1998; Prinz, 1992). The final age estimates are presented with their 1σ error in Table 1.

RESULTS

Structural Domains

For this study, the Camarillo fold belt was divided into five discrete structural domains, which characterize the highly segmented western extent of the Simi fault zone (Fig. 4B). Domain boundaries were defined by known and inferred north-striking cross faults (i.e., Barranca, Camrosa, Somis, and Wright Road faults), which juxtapose rocks having different composition, structural relief, orientation, and degrees of deformation (Fig. 4). From east to west, structural domains include: the Simi, Las Posas, Santa Rosa, Northern Springville, and Southern Springville domains (Fig. 4B). An additional structure located 5 km south of the main trace of the Simi fault, which is referred to here as the Camarillo fault, is discussed separately (Fig. 4B).

Simi Domain

This investigation includes only the western portion of what we refer to as the Simi domain, characterized by the Simi fault, which extends for ~7 km within the study area and ~12 km east of the study area (Fig. 2). The western boundary of the Simi domain is delimited by the north-striking Barranca fault, which juxtaposes pre-Quaternary strata on the east against folded Quaternary strata on the west (Fig. 4D). Within the study area, the Simi fault dips steeply (75°) northward at the surface and juxtaposes Miocene Conejo Volcanic and Topanga Formations (undifferentiated) in the footwall against the Simi anticline, which is developed in the Oligocene Sespe Formation (Fig. 4D). The Simi anticline plunges 15°–20° westward toward the Barranca fault. The Simi fault cuts the Barranca fault where it enters the Las Posas domain and appears to join with the southern Simi fault splay. There is no topographic expression of the Barranca fault north of the Simi anticline where it projects across the Qt2 terrace (Fig. 4D).

Las Posas Domain

The Las Posas domain is topographically characterized by the east-trending curvilinear

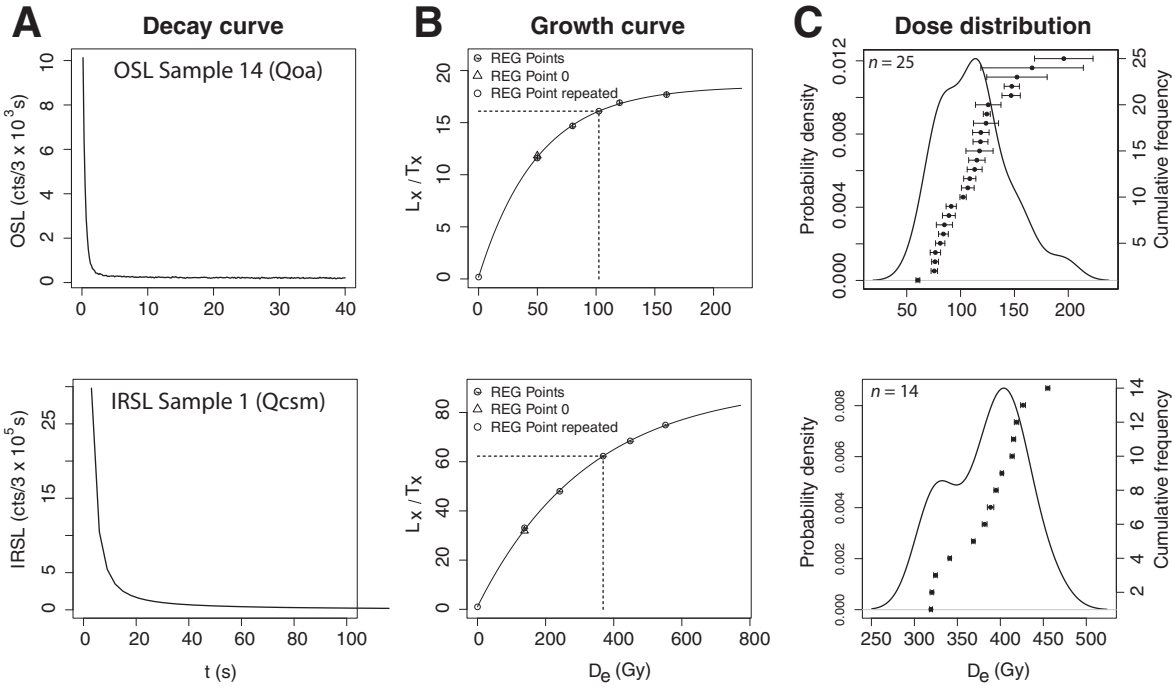

Figure 5. Examples of the luminescence characteristics of optically stimulated luminescence (OSL) and infrared stimulated luminescence (IRSL) samples. Typical OSL coarse-grain shine-down (A) and growth curves (B). (C) Dose distribution of aliquots with a probability density plot showing a positive skew and broad equivalent dose (D_e) distribution reflecting insufficient bleaching of some samples.

Las Posas anticline, defined by folded Las Posas Sand and Saugus Formations, which have IRSL ages of 141 ± 10 ka and 125 ± 9 ka, respectively (DeVecchio et al., 2012) (Fig. 4A). Paralleling the fold axis, the Las Posas domain is composed of several active and potentially active fault splays, including two northern segments and a concealed southern segment. The northern fault splays are exposed within the eroded hinge of the Las Posas anticline and are discontinuous right-stepping en echelon faults that approximate the location of the fold axis where the anticline trends west-southwest (Fig. 4B). Similar to the Oak Ridge fault and the Simi fault north of the Simi Valley, all fault splays within the Las Posas domain are inferred to have accommodated some component of Miocene dip-slip deformation based on thickness changes in Miocene Conejo volcanic rocks across the faults (Fig. 6A; Jakes, 1979; Hanson, 1980; Yeats, 1988b; this study). The northern fault splays dip steeply (75°–85°) to the north at the surface and predominantly juxtapose Miocene and older bedrock units, but, locally they offset the Las Posas and Saugus Formations. The southern Simi fault is largely concealed beneath younger alluvial-fan deposits along the front of the Las Posas Hills, but it has a dip of ~70° where it intersects borehole Shell Everett C-2 (#3 in Fig. 6A). Quaternary reactivation of the southern Simi fault is inferred based on offset of the base of Pleistocene strata in well logs (Fig. 6A), and a recent paleoseismic trench in the latest Pleistocene alluvial-fan sediments, which shows evidence of Quaternary faulting (Gurrola, 2008, personal commun.).

All splays of the Simi fault and the west-plunging Las Posas anticline terminate to the west (Jakes, 1979; Dibblee, 1992b) at a north-striking cross fault (Treiman, 1998) herein referred to as the Camrosa fault (Fig. 4C). Similar to the Simi fault splays, the Camrosa fault appears to have an older Miocene and younger Quaternary deformational history. The fault is manifested by: (1) the truncation of fault splays and folds to the east and west (Fig. 4C); (2) westward thickening of the Conejo-Topanga Formations across the fault (Fig. 7); (3) subsurface juxtaposition of the Sespe Formation to the east against Conejo-Topanga Formations to the west (Fig. 7); and (4) juxtaposition of the Qt2 surface on the west against Saugus strata on the east (Fig. 4C).

East of the Camrosa fault, the top of the Sespe Formation is exposed at an elevation of ~180 m above sea level (Fig. 7) and is overlain by a thin (5 m) veneer of Topanga strata that is capped by Las Posas Sand and the Saugus Formation (Fig. 4C). However, 200 m to the west across the Camrosa fault, subsurface well data show that the top of the Sespe Formation is 350 m below sea level and overlain by ~500 m of Topanga strata (Fig. 7). Post mid-Pleistocene transpressional deformation on the Camrosa fault is characterized by ~60 m of uplift of the base of the Las Posas Sand east of the Camrosa fault (Fig. 7).

Santa Rosa Domain

The Santa Rosa structural domain is bounded on its eastern margin by the Camrosa fault and on the west by Calleguas Creek (Fig. 4A), which occupies the location of the pre-Pleistocene north-northeast–striking Somis fault (Bailey, 1951; Jakes, 1979). However, Hanson et al. (2003) showed east-side-up displacement of early Pleistocene strata and eastward thinning of the Mugu aquifer across the Somis fault, suggesting late Quaternary activity. The southern part of the Santa Rosa domain is weakly folded and characterized by block uplift and northward tilting of the Qt2 surface in the hanging wall of the Santa Rosa Valley fault (Fig. 6B). In contrast, deformation along the Santa Rosa fault zone, to the north, is characterized by a diffuse zone of faulting and west-plunging folds (Fig. 4C). The topographic expression and displacement on the northern splay of the Santa Rosa fault splay (Fig. 6 of DeVecchio et al., 2012) are minimal and appear to only have been involved in deforming late Pleistocene strata. Therefore,

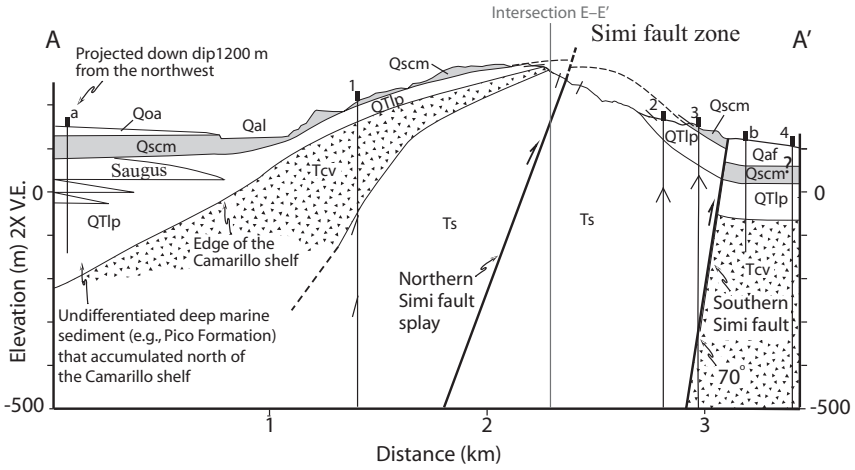

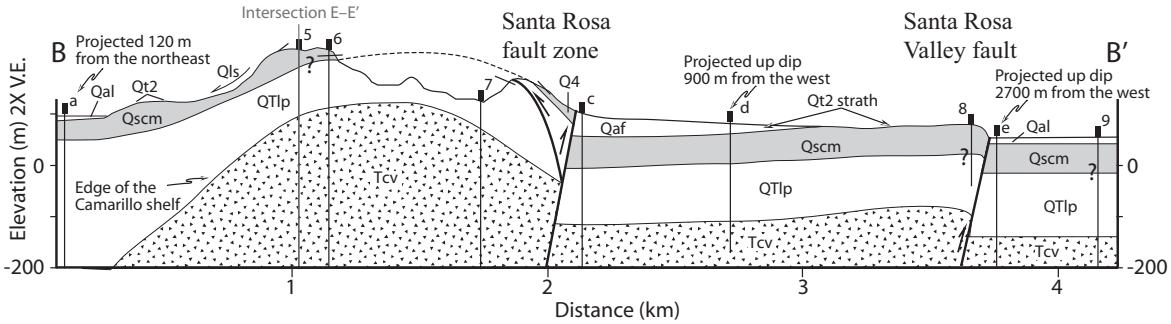

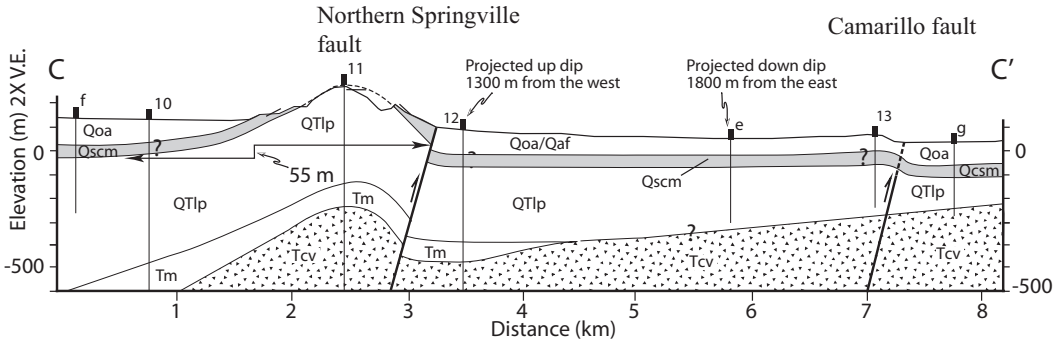

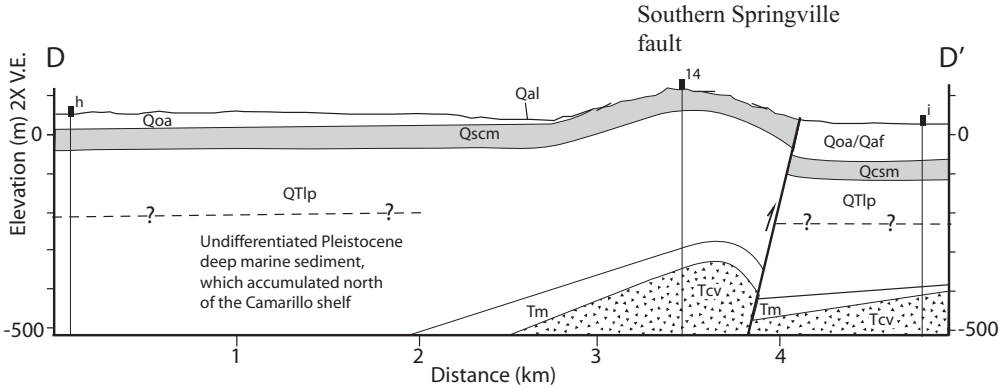

Figure 6. Four north-south–oriented cross sections across the Camarillo fold belt. See location of cross section lines (A–D) and explanation of geologic units on Figure 4. All sections have 2× vertical exaggeration and different horizontal scales. Lithologic interpretations of wells numbered 1–14 were taken from Jakes (1979), whereas interpretations of wells a–g are from Hanson et al. (2003). Queried Qscm contacts appear adjacent to wells of Jakes (1979), where differentiation of Upper Pleistocene units was not made; therefore, contacts are inferred based on projection from known depths. See Figure 4A legend for lithologic abbreviations. V.E.—vertical exaggeration. Well names: 1—Texaco Berylwood B-1; 2—Shell Everett 1; 3—Shell Everett C-2; 4—Exxon-Burket; 5—Aminoil-Burmah-Texaco Berylwood 1; 6—Burmah-Texaco Berylwood 3; 7— Texaco-Miketta 1; 8—A.J. Singer; 9—J. Schuck; 11—Arco McFarland 1; 12—Texaco-Converse 1; 13—Chevron Camarillo 1; 14—Reverse Schumate-Surpf; a—2N/21W-3B1; b—2N/20W-23H2; c—2N/20W-21L1; d—2N/20W-29B1; e—2N/20W-30M1; f—2N/21W-12H1; g—1N/21W-1B4; h—2N/21W-17F5; i—2N/21W-32E1.

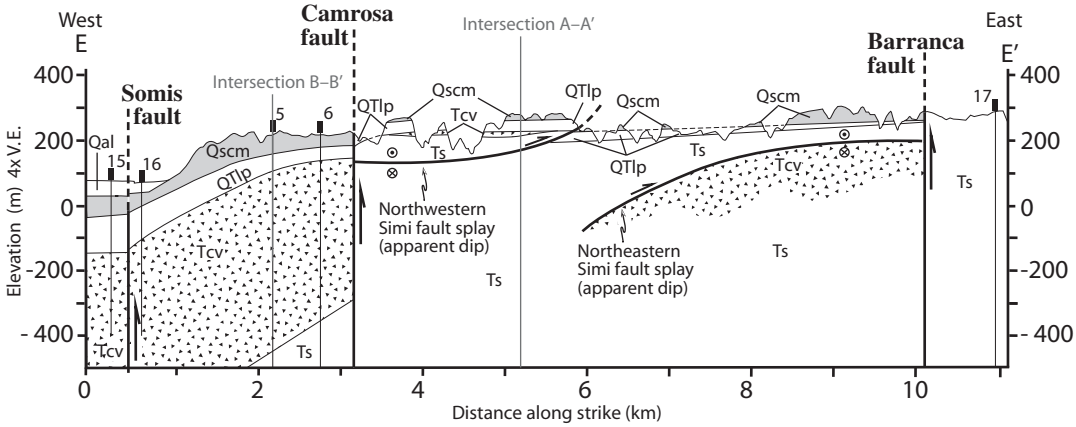

Figure 7. East-west cross section across the Simi, Las Posas, and Santa Rosa domains, illustrating the changes in structural relief and bedrock geology across north-striking cross faults. Note that structural relief of Qscm and the Sespe Formation decreases from east to west. See Figure 4A legend for lithologic abbreviations. See Figure 6 caption for well names 5 and 6. 15—Buttes Berylwood 1; 16—Buttes Berylwood 2; 17—Texaco Ventura Farms 1.

we interpret this structure to be a back thrust of the southern Santa Rosa fault, which has significantly more structural relief and underlies the zone of deformation (Fig. 6B).

The southern Santa Rosa fault juxtaposes Las Posas Sand and Saugus strata in the hanging wall against younger alluvial-fan sediments, which overlie the Qt2 surface to the south (Fig. 6B). Based on a radiocarbon age (Boales, 1991) and two OSL ages from sediments that overlie the Qt2 strath in three localities, the terrace has a weighted mean age of 24 ± 1 ka, while the base of the Saugus Formation in this domain has an IRSL age of 85 ± 6 ka (Table 1; Fig. 4A). The Santa Rosa folds show a westward decrease in topographic relief (Fig. 4B) and structural relief (Fig. 7), and together with limited surficial structural data (Fig. 4C), we infer that the Santa Rosa fold plunges westward toward the Somis fault. However, the anticline does not have an east-plunging limb and appears to be sutured to the west-plunging Las Posas anticline (Fig. 4C), similar to the Simi and Las Posas anticlines (Fig. 4D).

Northern Springville Domain

The northern Springville fault is bounded on its eastern side by the Somis fault and on its western side by an inferred north-striking fault. During preparation for the Spanish Hills urban development on the Camarillo Hills, Whitney and Gath (1991) documented abundant evidence of steep NE- and NW-trending tear faults with large lateral offsets near the eastern terminus of the southern Springville fault. Additionally, paleoseismic trenching within the accommodation zone between the Springville faults identified a subvertical N15E-trending fault for which the inferred trace approximately corresponds to the termination of both folds (Glenn, 1991). Based on these observations, the presence of two discrete left-stepping anticlines, and the different geomorphic expression and structural deformation of the folds (Figs. 2 and 4), we follow the interpretation of Jakes (1979) and consider the northern and southern Springville faults as discrete structural elements separated by a cross fault. We herein refer to the inferred north-striking cross fault as the Spanish Hills fault, which separates the northern and southern Springville domains (Fig. 4B).

Subsurface data from the northern Springville structural domain clearly show a westward change in bedrock stratigraphy. Specifically, the Las Posas Sand increases in thickness from 60 to 100 m in the Santa Rosa domain to more than 300 m in the Springville domain, and subsurface wells intersect the Miocene Monterey Formation (Tm) for the first time (Figs. 6B and 6C). These data suggest that the Camarillo shelf sloped northwestward during the Pleistocene, which resulted in preservation of the Monterey Formation and a thickened section of Las Posas Sand beneath the Springville domains. However, the Camarillo Member of the Saugus Formation exposed at the surface and in subcrop shows no change in thickness (Figs. 6C and 6D). An IRSL measurement from the base of the Saugus strata in the northern Springville domain gave an age of 78 ± 6 ka (Table 1; Fig. 4A).

Previous research on the northern Springville fault zone has resulted in different interpretations of fault dip. Based on subsurface data along the northern and southern Springville faults, Jakes (1979) argued strongly for a steeply north-dipping fault (70°–85°). However, based on a shallow test pit along the fault, Bailey (1951) suggested the fault dipped only 20°. We depict the fault as steeply dipping in cross section C–C′ (Fig. 6C) following Jakes (1979); however, because fault dip is critical to evaluating the magnitude of fault slip, a more thorough discussion of alternative fault dips in the Camarillo fold belt is included in the discussion section.

The south limb of the Camarillo Hills anticline is characterized by faceted spurs, steep to locally overturned Saugus strata on the southern forelimb, a gently dipping back limb (<20°) (Fig. 4A), and deeply incised drainages. Headward erosion of south-flowing drainages has driven the drainage divide north of the anticlinal axis and has exposed lower stratigraphic strata of the Las Posas Sand (Fig. 4A).

Southern Springville Domain

The southern Springville fault and anticline extends westward from Spanish Hills fault for ~4 km before abruptly terminating in the Oxnard Plain at the location of the Wright Road fault (Treiman, 1998) (Fig. 4B). Similar to the northern Springville domain, the Monterey Formation is preserved beneath a thick section of Pleistocene strata (Fig. 6D). Jakes (1979) also interpreted a steep dip (70°–85°) for the southern Springville fault based on subsurface data, whereas paleoseismic trenches suggest shallow subsurface dips of 15°–45° (Kile et al., 1991; Ruff and Shlemon, 1991; Gonzalez and Rockwell, 1991) (*see* Discussion section).

The Springville anticline in the hanging wall of the southern Springville fault is completely urbanized, and information about the geology and deformation is based largely on previous research during urban development. Previous researchers indicated that the degree of dissection was minimal before development and the

depth of erosion was limited to Saugus strata (McNamara et al., 1991). This is supported by digital elevation models (DEMs) created from predevelopment topographic maps (Fig. 2) and aerial photographs, which show that headward erosion of most drainages had not yet reached the crest of the fold, and the fold top was completely unincised, characteristic of an old geomorphic surface—potentially, the depositional top of the Camarillo Member of the Saugus Formation. Gonzalez and Rockwell (1991) suggested that the overlying surface had an age that was younger than 125 ka, supporting IRSL ages, which indicate that the Camarillo Member in this domain has an age of 85 ± 4 ka (Table 1; Fig. 4A). In contrast to the Camarillo Hills anticline, existing geologic maps show gentle bedding plane dips that are less that 25° on the forelimb and back limb of the fold (e.g., Dibblee, 1990).

Geochronology and Deformation of the Camarillo Anticline

The Camarillo fault, which lies ~4 km south of the northern Springville fault, is manifested by the 3-km-long, <25-m-high, east-trending Camarillo anticline, which plunges to the west beneath the Oxnard Plain (Fig. 4A). The topographic expression of the anticline is pristine in predevelopment aerial photographs and DEMs (inset, Fig. 8); however, the eastern part of the fold has likely been modified by Calleguas Creek (Fig. 2).

Three consulting paleoseismic trenches were opened across the forelimb of the Camarillo anticline for the purpose of locating the surface trace of the fault and to quantify the magnitude and timing of deformation. Trenches were logged by the managing consulting companies (Earth Systems Southern California, 2005; Geosoils Inc., 2006) and field checked during OSL sample collection to determine the depositional environment and stratigraphic context of numerical ages. Exposed in the uplifted hanging wall of the Camarillo anticline, the strata are composed of interbedded, well-sorted, cross-bedded fluvial sand, moderately sorted pebble gravel, and massive clay-rich overbank deposits. Both the Earth Systems and Geosoils, Inc., trench logs give the name Saugus Formation to tilted and faulted strata; however,

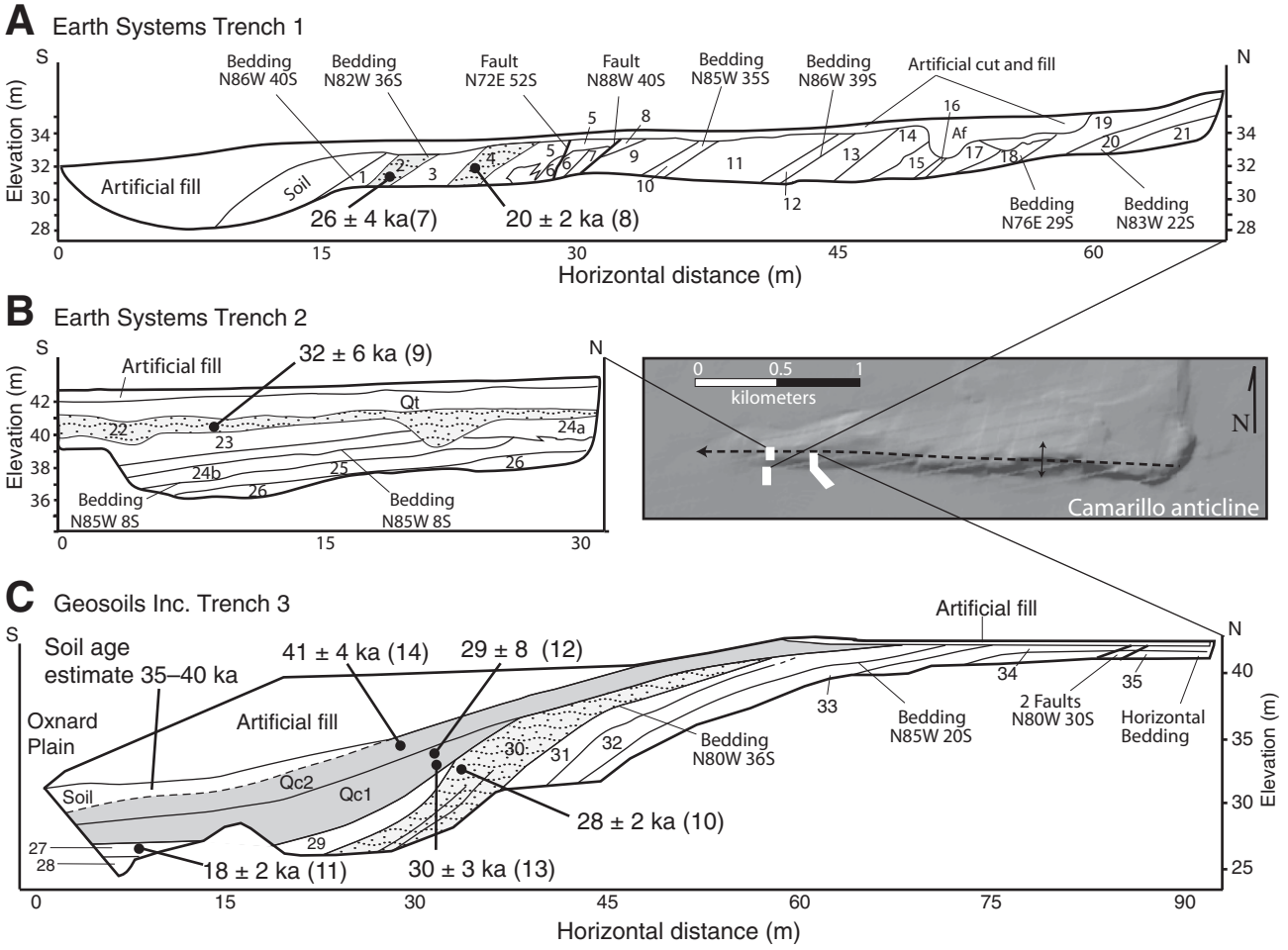

Figure 8. Simplified line drawings of consultant trench logs across the Camarillo anticline. Inset shaded relief map shows the relative position of fault trenches with respect to the axis and topographic expression of the Camarillo anticline. See Figure 4 for the location of the Camarillo anticline. Numbered units (1–35) are an interbedded sequence of well-sorted fluvial gravel, sand, and silt beds referred to as Saugus Formation in consultant logs (Qoa, this study). (A) Optically stimulated luminescence (OSL) samples were dated from two stratigraphic horizons of Qoa. Minor back thrusting was observed, but the Camarillo fault was not encountered. (B) Trench 2 was opened near the crest of the fold and showed evidence of post-tectonic erosional bevelling. A single OSL sample was collected from below an unconformable terrace deposit (Qt). (C) Three OSL samples were collected from Qoa strata and two colluvial wedge units (Qc1 and Qc2), which are discordant with the underlying fluvial strata and are interpreted to record post-tectonic deposition on a growing fold. Minor back thrusting and bedding plane shearing was observed, but the Camarillo fault was not definitively encountered. Note, trench C is not the same scale as trenches 1 and 2.

Jakes (1979) and Dibblee (1992a) referred to these strata as older alluvium (Qoa) (numbers 1–35 on Fig. 8). Because these sediments overlie the Camarillo Member of the Saugus Formation (Fig. 6C), we use the name older alluvium (Qoa); however, because the Saugus Formation is poorly defined (DeVecchio et al., 2012), these sediments may be lithostratigraphically correlative with the Saugus Formation mapped elsewhere.

Trench 1 was excavated in a former gravel pit, which explains the upward truncation of stratigraphic horizons 1 through 19 and overlying artificial fill (Fig. 8A). The beds dip as much as 40° to the south and show some evidence of minor hanging-wall deformation, including extensional and compressional faulting and bedding plane shearing (Earth Systems Southern California, 2005). OSL samples were collected from two discrete sandy stratigraphic horizons separated by 1.5 m within the trench and gave ages of 26 ± 4 ka and 20 ± 2 ka (Fig. 8A; Table 1, samples 6 and 7).

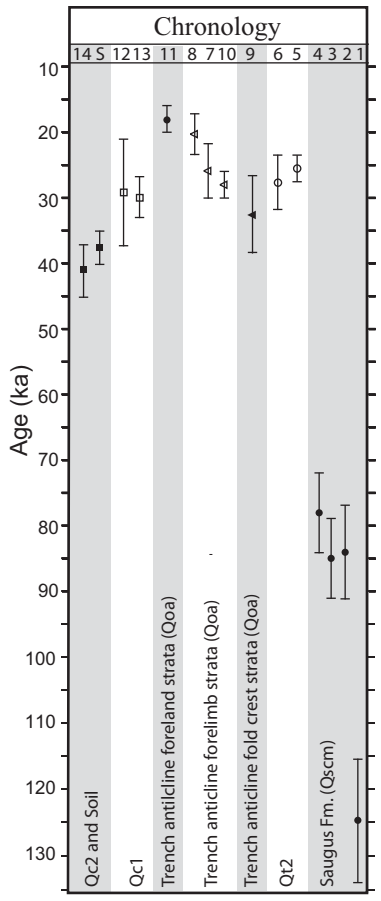

Figure 9. Age control summary showing the distribution of ages used to assess the timing and rates of deformation in the Camarillo fold belt (CFB). Numbers across the top correspond to the sample numbers shown on Table 1.

A single OSL sample was collected from trench 2, which was opened on the crest of the fold near the anticlinal axis. The sample was collected from a gently southward-dipping bed (<10°; Fig. 8B) and gave an age of 32 ± 6 ka (Table 1, sample 9). The older age near the crest compared to forelimb strata exposed in trench 1 suggests that surface beveling of the anticline occurred during uplift, which exposed deeper stratigraphic units along the locus of uplift. Erosion of the crest is supported by a gravel horizon that unconformably overlies bed 22, which Earth Systems Southern California (2005) interpreted to be an unconformable terrace deposit (Qt on Fig. 8B).

Trench 3 was located ~100 m east of the Earth System trenches and was excavated across the entire forelimb of the Camarillo anticline (Fig. 8C). Beds dip as much as 36° in the southern part of the trench and are almost flat lying in the northernmost exposure of the trench. Stratigraphic horizons 29 through 34 are upwardly truncated, which indicates that as much as 20 m of the Qoa strata were eroded from the forelimb and crest of the fold during uplift. Forelimb strata are overlain by two colluvial wedge deposits (Fig. 8C, Qc1 and Qc2). The upper colluvial wedge (Qc2) has an inferred age of 35–40 ka based on a soil age estimate (Geosoils Inc., 2006). Similar to trench 1, the Camarillo fault was not definitively encountered in trench 3. These results support previous paleoseismic investigations conducted ~1.5 km to the east, which suggested that the Camarillo fault is blind along its entire length (Yeats et al., 1997).

Four OSL samples were collected and dated from three stratigraphic horizons in trench 3 (Fig. 8C). The lowermost sample was collected from tilted forelimb strata (bed 30) composed of cross-bedded sand and gave an age of 28 ± 2 ka (Table 1, sample 10). A second sample was collected from flat-lying fluvial sands of the Oxnard Plain in the foreland of the Camarillo anticline and gave an age of 18 ± 2 ka (Table 2, sample 11). Three samples were analyzed from Qc1 and Qc2, which gave internally stratigraphically inconsistent ages, with the upper deposit giving the oldest age of 41 ± 4 ka, whereas the underlying samples gave ages of 28 ± 2 ka and 30 ± 3 ka. Moreover, age results from colluvial wedge deposits are stratigraphically inconsistent with all other fluvial strata deformed in the forelimb of the fold and present in the Oxnard Plain sediments, which underlie the colluvial deposits (Table 1).

DISCUSSION

This research, together with that by DeVecchio et al. (2012), provides new insights into the paleogeography and the erosional and depositional processes that shaped the landscape in this region of the Western Transverse Ranges. These processes have been modulated by late Pleistocene climate, as well as local tectonics. Our geochronology, and structural and stratigraphic analyses enable us to reconstruct the landscape evolution of the region, and correlate deformed sedimentary strata to better interpret geochronological results in order to minimize error in quantifying Quaternary deformation rates.

Geochronology

The robustness of the OSL results from Pleistocene strath terraces and the IRSL results from the Camarillo Member of the Saugus Formation are supported by terrestrial cosmogenic nuclide and radiocarbon ages, which are within error of the results presented here (DeVecchio et al., 2012). However, OSL results from paleoseismic trenches across the Camarillo anticline are more complicated and require additional discussion.

Collectively, the OSL ages from fluvial strata deformed in the forelimb of the Camarillo anticline record deposition between ca. 30 ka and ca. 20 ka, which is stratigraphically inconsistent with older ages that come from overlying colluvial wedge deposits and an age-dated soil (Fig. 9). Anomalously young OSL ages are not expected, as partial bleaching of quartz grains before deposition should result in age overestimates (i.e., Aitken, 1998). There are two possibilities that may explain age underestimates of the fluvial strata. One possibility is that all of the samples were contaminated by younger grains that were transported downward by bioturbation or plant roots. However, contamination of four samples collected from three different localities seems unlikely. In addition, we saw no evidence of these processes in the well-bedded fluvial sediments exposed in the trench walls. However, if the assumed water content used to assess the sediment ages (15%) underestimates the actually water content of the sample since the time of burial, OSL ages may underestimate the actual depositional age of the fluvial strata. This is a possibility, because prior to uplift, these sediments would have been part of the upper aquifer system, which is partially saturated in this part of the Oxnard Plain (Hanson et al., 2003). This likely explains why sample 11, from the foreland of the fold, within the modern Oxnard Plain, gave a somewhat younger age compared to other Qoa sediments in the trench based on the same assumed water content (Table 1; Fig. 8). Furthermore, we would not expect Qc1 and Qc2 to have been affected by this same issue because they were deposited above the saturated zone

TABLE 2. MAGNITUDES AND RATES OF DEFORMATION

Fault name	Structural domain	Total uplift (m)	Fault uplift (m)	Fold uplift (m)	Fault slip (m)	Shortening (%)	Age range of offset datum (ka)	Fault slip rate range (mm/yr)*	Total uplift rate range (mm/yr)*	Shortening rate range (mm/yr)*
Simi	Simi		24		26		23–25†	1.0–1.1		
Southern Simi (long-term)	Las Posas	297	97	200	104	5	116–134§	0.8–0.9	2.2–2.5	0.8–1.0
Southern Simi (short-term)			24		26		23–25†	1.0–1.1		
Southern Santa Rosa (long-term)	Santa Rosa	225	78	147	83	3	78–86#	1.0–1.1	2.6–2.8	0.7–0.8
Southern Santa Rosa (short-term)			25–30		27–32		23–25†	1.1–1.4		
Santa Rosa Valley	Santa Rosa	30	30	0	32		23–25†	1.3–1.4††	1.2–1.3††	
Northern Springville	No. Springville	356	92	264	98	6	78–86#	1.1–1.3	4.1–4.6	1.7–1.8
Southern Springville	So. Springville	174	74	100	78	4	78–86#	0.9–1.0	1.9–2.2	0.6–0.7
Camarillo		45					26–40**	N/A	1.1–1.7	

Note: Gray boxes represent compound systems discussed in text.
*Rate estimate represents minimums where based on the age of Qcsm and Qoa, which is always older than the timing of tectonic deformation.
†Age of the Qt2 surface based the weighted mean of two optically stimulated luminescence (OSL) dates (Table 1) and a single radiocarbon age DeVecchio et al. (2012).
§Age range estimate based on infrared stimulated luminescence (IRSL) age and associated error on deformed Qscm strata within the Las Posas domain (see Fig. 4A; Table 1).
#Age range estimate based on the weighted mean of three IRSL ages from the base of Qscm west of the Camrosa fault (see Fig. 4A; Table 1).
**The upper age limit is based on the minimum possible age of the soil and the minimum age of OSL samples from the forelimb of the anticline assuming a water content of 50%, whereas the lower age is based on the maximum age of the soil (see text for discussion).
††Rate estimate is a maximum because deformation began before the Qt2 strath was cut (see text for discussion).

following uplift. However, even if fluvial strata in the forelimb had a porosity of 50%, which is greater than what we determined but is possible for well-sorted sands, forelimb strata would all still have ages of less than 35 ka, and most of the fluvial strata would still have ages younger or coeval with the overlying Qc2 and soil (Fig. 9). Alternatively, ages of the overlying colluvial sediments may be too old.

There are several good reasons to suspect that the OSL ages of samples collected from Qc1 and Qc2 were affected by insufficient bleaching and, therefore, likely represent age overestimates. Colluvial wedge deposits were likely derived from slope failure along the crest of the growing Camarillo anticline (Geosoils Inc., 2006). In this case, the dated quartz grains collected from Qt1 and Qt2 may not have been exposed to sunlight during mass transport down the forelimb of the fold (*see* Murray and Olley, 2002). Therefore, the ages of dated grains reflect the age of lower stratigraphic units, such as sample 9, exposed along the crest of the anticline at the time of Qc1 and Qc2 deposition (Fig. 9). This is well supported by the massive character of the colluvial deposits and evidence of erosion along the crest of the fold before deposition of Qc1 and Qc2 (Fig. 8). In addition, this interpretation also explains the inverted stratigraphic ages of Qc1 and Qc2, which would be expected as deeper stratigraphic units were exposed along the fold crest through time.

Assuming an OSL age overestimate of the colluvial deposits, it must be concluded that the soil age is also an age overestimate, which is possible since soil age estimates are qualitative and at best have an uncertainty of ±25% (e.g., Keller and Pinter, 2002). Although still older than sample 8 (20 ± 2 ka) in the forelimb and sample 11 from the foreland (18 ± 2 ka), a soil age of ca. 26 ka (−25% of 40 ka) would be stratigraphically consistent with other samples from the paleoseismic trenches. In order for all samples to be within error of the soil ages estimate, however, a water content of 30% for sample 8 and 50% for sample 11 would need to be assumed (Fig. 9), which is plausible but higher than expected. In addition, tectonic folding and deposition of the both colluvial wedge deposits would need to have occurred rapidly following deposition of fluvial strata.

Although it is less complicated to explain OSL age overestimates from the colluvial deposits than to explain age underestimates from the fluvial strata, based on the soil age estimate we are forced to assume that some of the OSL ages from the fluvial strata are potentially too young. This is surprising because both OSL and IRSL samples collected elsewhere in the Camarillo area are in good agreement with other numerical techniques (DeVecchio et al., 2012). Consequently, we assign a broad age range (40–26 ka) to deformed sediment exposed in the trenches to be used for estimating the timing and rate of deformation along the Camarillo anticline (Table 2). An upper age limit of 26 ka is assumed based on the minimum possible age of the soil and the minimum age of OSL samples assuming a water content of 50%, whereas the lower age of 40 ka is based on the maximum age of the soil age estimate.

Kinematic Analysis

Quaternary deformation within each of the structural domains was estimated from cross sections shown in Figure 6. We differentiated among fault slip, total uplift, uplift due to faulting, and uplift due to folding to illustrate the ways in which strain is accommodated (Fig. 10). The magnitudes of these variables are shown in Table 2. With the exception of the northern Springville fault, which has ~55 m of differential hanging-wall uplift (Fig. 6C), hanging-wall uplift in response to faulting is approximately constant perpendicular to the fault (Fig. 10, line BE is horizontal). Uplift due to folding is typically twice that of uplift due to faulting (Table 2). Folding is interpreted to be the result of local-

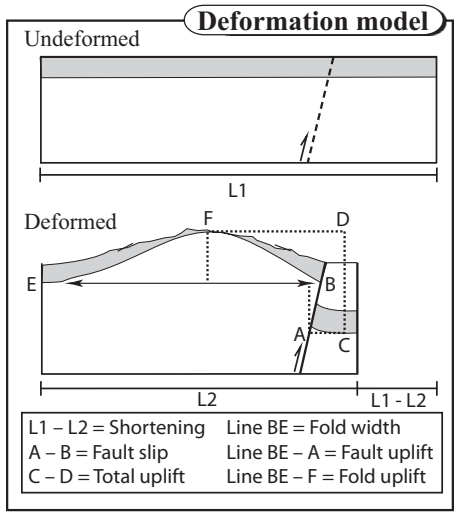

Figure 10. Illustration of methods used to estimate different variables of deformation shown on Table 3. With the exception of the northern Springville fault, hanging-wall uplift is constant and perpendicular to the fault (line BE is horizontal), indicating that fault dip remains constant, and hanging-wall folding adjacent to the bounding fault is the result of local deformation and does not characterize uplift due to faulting.

ized deformation adjacent to the fault and not fault propagation folding because most faults in the study area are inherited structures that were within the upper few hundred meters of the surface when contractional deformation began. Therefore, estimates of fault slip are derived from line AB (Fig. 10) and not from the structural relief of the anticlines (Fig. 10, line CD).

Perhaps one of the most critical unknowns and the most controversial aspect of the deformation in the Camarillo fold belt is whether or not faults represent discrete seismic sources. Faults may be aseismic if they dip gently or if they are detached in the shallow subsurface in weak Pliocene–Pleistocene strata (Rockwell, 2008, personal commun.) and intersect the Oak Ridge fault before encountering high-strength rocks capable of accumulating significant amounts of elastic strain (Gonzalez and Rockwell, 1991). In the following paragraphs, we briefly discuss this possibility.

The main reason for suspecting that faults in the Camarillo fold belt are kinematically linked to the Oak Ridge fault comes from gentle dips encountered in paleoseismic trenches along the southern Springville fault (Gonzalez and Rockwell, 1991), and from faults and folds in the Ventura fold belt (Fig. 1), which have been shown to be detached at shallow depths (5 km) within a thick section of weak Miocene and Pliocene–Pleistocene sedimentary bedrock (Yeats, 1981, 1983; Huftile and Yeats, 1995). We are confident that the Camarillo fault and faults in the Simi, Las Posas, and Santa Rosa domains are not detached within weak bedrock because Neogene sedimentary bedrock is absent, and only a thin veneer (<100 m) of late Pleistocene strata is present (Fig. 6). Although this does not preclude the possibility of gentle fault dips in the pre-Pleistocene bedrock, the preponderance of surface and subsurface evidence from these structural domains indicates that most of the Quaternary faults in the Camarillo fold belt are reactivated high-angle Miocene faults. The degree to which faults flatten at depth is difficult to assess; however, the uniform uplift of the hanging-wall blocks in our cross sections, which are constrained by subsurface data, does not support a shallowing of fault dip at depth. Although the dip of the Camarillo fault is less well constrained, we similarly infer a fault that cuts deeply into high-strength rocks based on its position on the Camarillo shelf with respect to Conejo volcanic rocks in the shallow subsurface (Fig. 6C).

In contrast to other structural domains, the Springville fault zone was located near the shelf break, where a considerably thicker section of Pliocene–Pleistocene marine strata accumulated above the Miocene Monterey Formation (Figs. 6C and 6D). The Monterey shale is a weak bedrock horizon where deformation could become localized (i.e., Yeats, 1983) above the Conejo volcanics. Figure 11 illustrates an alternative cross section across the northern Springville fault where the fault dips gently and displacement becomes localized in the Monterey Formation at depth. In this model, the Springville fault would need to dip at ~25° in the upper few hundred meters of the surface to intersect the Monterey Formation and flatten to a dip of ~10° at a depth of 500 m below sea level (Fig. 11). In this case, the northern Springville fault would intersect the Oak Ridge fault in the upper 3 km of the crust, which is well above the depth of most seismicity greater than M_w 5.0 in the region (SCEC Earthquake Data Center, 2011).

A fault bend fold model, such as the one shown in Figure 11, could explain the differential uplift of the northern Springville hanging wall; however, the reconstruction is problematic. Due to the more gentle dip of the fault in the upper 100 m of the surface, ~88 m of differential hanging-wall uplift would be expected. Although this is greater than the observed differential uplift (55 m) estimated from cross section C–C′ (Fig. 6C), it does support a flattening of the northern Springville fault at depth. However, in order to reconstruct the subsurface geometry of the Monterey Formation encountered by wells 11 and 12, several assumptions are required. Well 11 intersects the Monterey Formation at a depth of ~150 m below sea level, whereas in well 12, the Monterey Formation is at a depth of 400 m. This is not consistent with the northward dip of the Monterey Formation observed in all subsurface wells and other cross sections across the region (Fig. 3). Therefore, in order to balance the cross section in Figure 11, there would need to be at least 250 m of post-Miocene pre-Saugus folding and/or faulting beneath the northern Springville fault footwall (Fig. 11), which is not supported by subsurface or surface geologic relations beneath either of the Springville domains. In addition, fault dips of 10°–25° would yield fault slip rates of >5 mm/yr, which is five times greater than estimates from paleoseismic studies (Gonzalez and Rockwell, 1991) and seems excessive. Therefore, we interpret the Springville fault zone to be characterized by steeply dipping faults that cut deeply into high-strength rocks, and therefore represent discrete seismic sources similar to other faults in the Camarillo fold belt that are not kinematically linked the Oak Ridge fault.

Deformation Rate Calculations

We are confident that most of the rates shown on Table 2 represent minimums because rate estimates are based on the ages of folded and faulted depositional deposits (Saugus and Qoa), and not the actual onset of deformation, which began sometime following deposition. Because Saugus ages west of the Camrosa fault are all within error (Table 1; Fig. 10), we assume that progradation of terrestrial strata was rapid across this part of the shelf and, therefore, use the weighted mean of these three ages (82 ± 4 ka) to estimate long-term rates of deformation within the Santa Rosa and Springville domains (Table 2). However, within the Las Posas structural domain, the age of the Camarillo Member of the Saugus Formation is ~30% older than strata deformed to the west (Table 1). If we utilize this older Saugus age to estimate deformation rates, we get long-term rates for the southern Simi fault that are relatively low, even though the total deformation within the Las Posas domain is greater than that of most of the other structural domains (Table 2). To test long-term uplift rates based on the Saugus Formation, we compared results from short-term uplift rates estimated from separation of the Qt2 strath and Calleguas Creek, which DeVecchio et al. (2012)

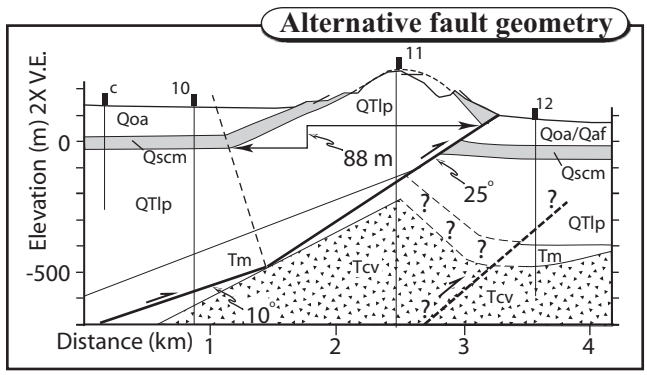

Figure 11. Alternative cross sections across the northern Springville fault showing the fault dipping gently in the shallow subsurface, and flattening and becoming localized within the Monterey Formation (Tm) at depth. The Springville anticline is depicted as a fault bend fold, which is estimated to produce ~88 m of differential hanging-wall uplift. Previously unknown faulting and/or folding of the Springville footwall is required to balance the section based on the bedrock geology encountered in wells 11 and 12, and, therefore, this section fault geometry is not preferred (see text for discussion). See Figure 4A for lithologic abbreviations. V.E.—vertical exaggeration.

suggested were genetically related. Because the Saugus Formation was not preserved or was not deposited before uplift of the Simi anticline, we relied exclusively on incision of the Qt2 strath in the Simi domain to estimate fault-related hanging-wall uplift, which indicates a short-term uplift rate of 1.0–1.1 mm/yr (Table 2). This result agrees with a previous paleoseismic studies within the domain (Hitchcock et al., 1998).

The magnitudes of fault slip beneath the large anticlines in the study area (Las Posas, Santa Rosa, Camarillo Hills, and Springville anticlines), which lie along the main trace of the Simi fault, are remarkably similar (78–104 m). Consequently, long-term fault slip rates along the study area are similar (0.8 mm/yr to 1.4 mm/yr; Table 2). Within the Las Posas and Santa Rosa domains, where the Qt2 surface is preserved, short-term (<23–25 ka) rate estimates overlap with longer-term rate estimates, but are slightly greater (Table 2). The greater short-term rates support the argument that rates based on the age of deformed Saugus strata represent minimums, in which case, short-term rates likely represent a better estimate of actual uplift rates. Regardless, long-term and short-term rate estimates agree reasonably well, suggesting that hanging-wall uplift rates have remained fairly constant, and, therefore, we infer a long-term uplift rate of 1.0 mm/yr on the Simi fault from short-term estimates within the Simi domain. Fault slip rates shown in Table 2 overlap with, but are locally greater than, previous estimates from paleoseismic investigations.

Folding and uplift of the Santa Rosa Valley hanging wall began sometime before the Qt2 strath was cut, based on upward truncation of Saugus strata that dip gently (<5°) north beneath Qt2. Because deformation began before beveling of the strath, uplift rate estimates derived from the age of Qt2 represent a maximum. We measured ~30 m of post-Qt2 uplift adjacent to the fault based on the separation of the Qt2 strath and Calleguas Creek. Subsurface data from the base of the Saugus Formation near the southern Santa Rosa fault indicate that uplift of the Santa Rosa Valley hanging wall decreases to the north to 10–15 m (Fig. 6B, well c). Based on the age of the Qt2 surface, we estimate a maximum uplift rate adjacent to the fault of 1.2–1.3 mm/yr (Table 2). However, if the onset of deformation was contemporaneous with other structural domains to the north, then late Pleistocene uplift rates for the Santa Rosa Valley fault would be relatively low compared to other faults (0.3–0.4 mm/yr). Based on the minimal amount of angular discordance between the Saugus strata and the overlying Qt2 strath, we interpret the Santa Rosa Valley fault to be more youthful than faults to the north and to be characterized by similar fault slip rates (~1.0 mm/yr).

Deformation along the Camarillo fault appears to be similar in age to that of the Santa Rosa Valley fault, having begun ca. 26–40 ka. Uplift estimates for the Camarillo fault are derived from exposures in the paleoseismic trenches shown in Figure 8. Because the Camarillo fault is blind, and we are unable to correlate older alluvial deposits across the fault in the subsurface, we do not estimate fault slip but rely upon total uplift to assess deformation. The total uplift is estimated from the sum of structural relief of Qoa sediments in the trench (15 m) and the eroded thickness (20 m) from the fold crest. This suggests ~35 m of uplift related to fault propagation folding at the westernmost surface exposure of the Camarillo anticline. If a similar amount of erosion occurred along the crest near the topographic high point of the fold, 1.5 km to the east, total vertical uplift may be as high as 45 m. This suggests a total uplift rate of 1.1–1.7 mm/yr, which is similar to the Santa Rosa Valley fault but less than faults along the trend of the Simi fault zone (Table 2).

Although lower than the fault slip rate on the Oak Ridge fault, rates in the Camarillo fold belt are comparable to rates documented on other potentially hazardous contractional fault systems in Southern California, including: Santa Monica, Elysian Park, Puente Hills, and Santa Barbara (Dolan et al., 2000; Oskin et al., 2000; Shaw et al., 2002; Keller and Gurrola, 2000; Fig. 1). Perhaps the most interesting factor is that such a well-developed fold belt could grow in less than 125 k.y. This is likely the result of high rate of folding adjacent to the active faults, which is two to three times greater than uplift due to faulting (Table 2). If this style of deformation is common in other fold belts, fault slip estimates based on uplift across anticlinal folds may overestimate the true magnitude and rate of fault slip.

Temporal Patterns of Fold Growth

By comparing adjacent structural domains where folds have grown together into a single topographic feature, such as the Simi and Las Posas domains with the Santa Rosa domain, and the northern Springville with the southern Springville domain, we can make some interesting observations about the spatio-temporal patterns of deformation. The two compound systems considered are shown in the two gray boxes on Table 2. Although Saugus strata are not preserved in the Simi domain, we infer that the Simi anticline has the greatest magnitude of Quaternary uplift and shortening based on the greater structural relief of the Sespe Formation (Fig. 7). In which case, all measured magnitudes of long-term uplift and shortening decrease from east to west within the two compound systems. In addition, a westward decrease in the magnitude of forelimb rotation occurs across intervening cross faults (Fig. 4A). These observations indicate that either the long-term deformation rates decrease toward the west or the timing of local deformation is younger toward the west.

We utilize incision of the Qt2 strath preserved within the Simi–Las Posas–Santa Rosa system to assess strike-parallel timing and rates of deformation within these domains. Separation between Qt2 and Calleguas Creek is constant at ~24 m within the Simi and Las Posas domains (Fig. 12), suggesting similar rates of post-Qt2 fault-related uplift for the two domains. If the assumption that long-term rates have

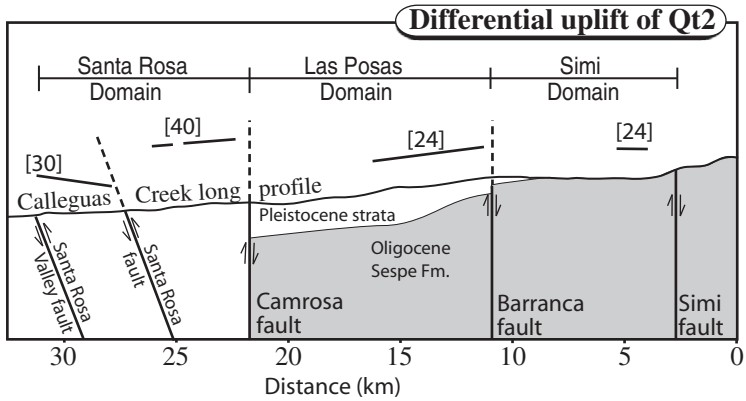

Figure 12. Long profile of Calleguas Creek with respect to the Qt2 strath. Separation, in meters, between Qt2 and Calleguas Creek is shown in brackets. Separation is constant within the Simi and Las Posas domains, indicating that post-Qt2 hanging-wall uplift rates are similar across the Barranca fault. The greater magnitude of separation west of the Camrosa fault suggests that post-Qt2 uplift rates are greater in the Santa Rosa domain than in structural domains to the east (see text for discussion).

remained constant is valid, then we can infer from the greater structural relief (~20 m) in the Simi domain that deformation in the Las Posas domain is ~20% younger. This may explain the absence of deformed Saugus strata across the Simi anticline and the eastward pinching out of the Las Posas Sand (Fig. 4D), if deformation in the Simi domain began before deposition of the Las Posas Sand at ca. 140 ka (DeVecchio et al., 2012). A similar and more compelling argument can be made for the timing of deformation between the Las Posas and Santa Rosa domains, where after crossing the northward projection of the Camrosa fault, incision into Qt2 increases from 24 m to 40 m (Fig. 12). The increase in separation is not coincident with any change in the long profile of Calleguas Creek, bedrock lithology, or any significant confluence within the river network, and therefore is interpreted to be the result of greater uplift rates within the Santa Rosa domain. Northward tilting of the Santa Rosa Valley hanging wall (Fig. 6B) suggests that 25–30 m of the uplift west of the Camrosa fault can be attributed to uplift of the southern Santa Rosa fault, signifying a short-term uplift rate of 0.9–1.3 mm/yr on the southern Santa Rosa fault (Table 2). Because the rates in the Santa Rosa domain are similar to or greater than those of the domains to the east, yet the magnitude of deformation is less, we infer that the onset of deformation is younger toward the west. Changes in uplift magnitude and rate, structural style (Fig. 4), and structural relief (Fig. 7) appear coincident with the north-striking faults, which suggests that cross faults have strongly influenced the kinematic evolution of the fold belt and the timing of westward growth of the Simi fault system (*see* Punctuated Lateral Fault Growth section).

There are less direct data from the Springville fault pair; however, similar observations suggest that this fold complex may have a similar evolution to that of the Simi–Las Posas–Santa Rosa system. Specifically, we interpret the westward decrease in forelimb rotation, hanging-wall erosion, and magnitudes of uplift and shortening (Table 2) for the Springville anticline to reflect a younger age than that of the Camarillo anticline to the east, rather than a lower rate of deformation.

Punctuated Lateral Fault Growth Model

In the previous discussion, we interpreted structural domains to be discrete deformation zones isolated by north-striking cross faults, which have controlled the styles, timing, and magnitudes of deformation. However, based on structural trends and local fault offsets, we propose that some of the structural domains have grown together, and faults that were once discrete structural elements have been become linked across domain boundaries. The most apparent example of this is the linkage of the Simi and Las Posas domains across the Barranca fault (Fig. 4B). Although the Barranca fault truncates the northern Simi fault on the west and the Simi anticline on the east, the Barranca fault is cut by and offset across the southern Simi fault system (Fig. 4D). Although the Camrosa fault does not appear to be similarly offset, based on the magnitude of deformation on the southern Simi and southern Santa Rosa faults, similar slip rates, and collinear traces across the Camrosa fault, we suggest that the Simi and Santa Rosa faults may now be linked. The interpretation that the Simi fault is a single structural element that extends from the Simi Valley to Calleguas Creek is not unique to this study and has been suggested by most previous research along this section of the fault (Jakes, 1979; Dibblee, 1992b; Treiman, 1998).

The westward decrease in structural relief that occurs across the Barranca and Camrosa fault (Fig. 7), and the evidence of westward younging of structural domains (*see* previous discussion) suggest that the Simi fault system is growing westward out of the Simi Valley into the Camarillo area. Figure 13 illustrates recent fault growth models. In compressional tectonic settings, all three models results in a hanging-wall anticline that plunges in both directions; however, complex folding may occur where propagating anticlines have become sutured (Fig. 13C). In contrast, folds within the Camarillo fold belt are characterized by only west-plunging fold axes, and few east-dipping bedding attitudes have been mapped in the region (e.g., Jakes, 1979; Hanson, 1980; Dibblee, 1992a, 1992b).

To explain the westward younging from of the Simi–Las Posas–Santa Rosa system, the absence of east-plunging fold axes, and the westward decrease in structural relief across north-striking cross faults, we suggest a model whereby westward growth of the Simi fault occurs by punctuated lateral propagation (Fig. 14). The model incorporates elements of both the constant-fault-length and increasing-fault-length models (Figs. 13A and 13B).

Initial folding and uplift in the Camarillo fold belt began in the Simi domain and likely farther to the east north of Simi Valley (Fig. 2) before propagating westward. Westward growth of the Simi fault at "time 1" (Fig. 14) was limited by the Barranca cross fault, which resulted in amplification of the west-plunging Simi anticline under constant-fault-length conditions (Fig. 13A). Strain gradients near the fault-fold tip, adjacent to the Barranca fault, likely built with incremental displacement on the fault until stress became critical, and the Simi fault was

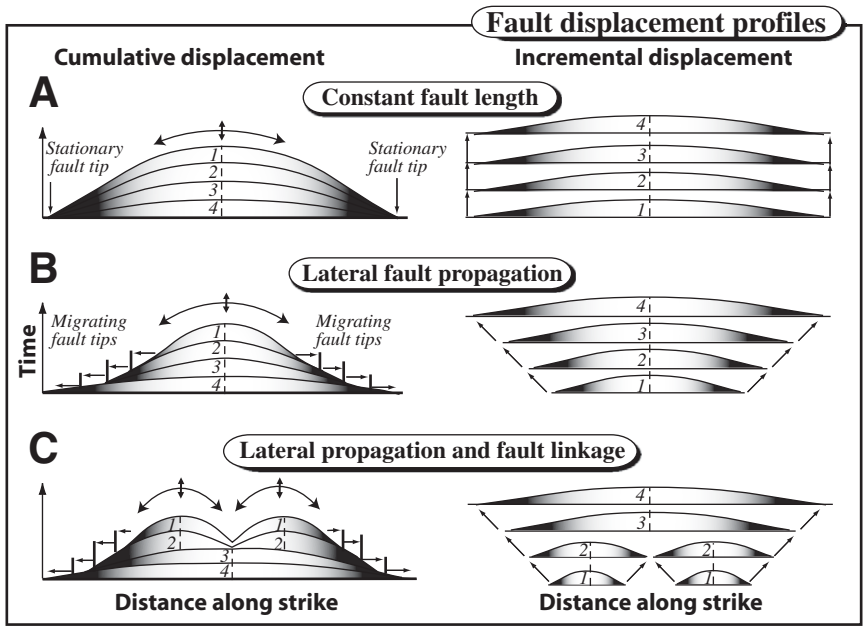

Figure 13. Hypothetical along-strike displacement profiles for fault growth (A) at a constant length, (B) with increasing fault length through lateral fault tip propagation, and (C) by fault linkage of laterally propagating fault segments (modified from Nicol et al., 2005). For A and B, the summation of the incremental growth (1–4) results in a stationary locus of maximum uplift within the cumulative profiles (dashed line). For the fault linkage model, the locus of maximum uplift would migrate to the center of the sutured structures beginning at time 3 and would remain constant and stationary until another linkage occurred.

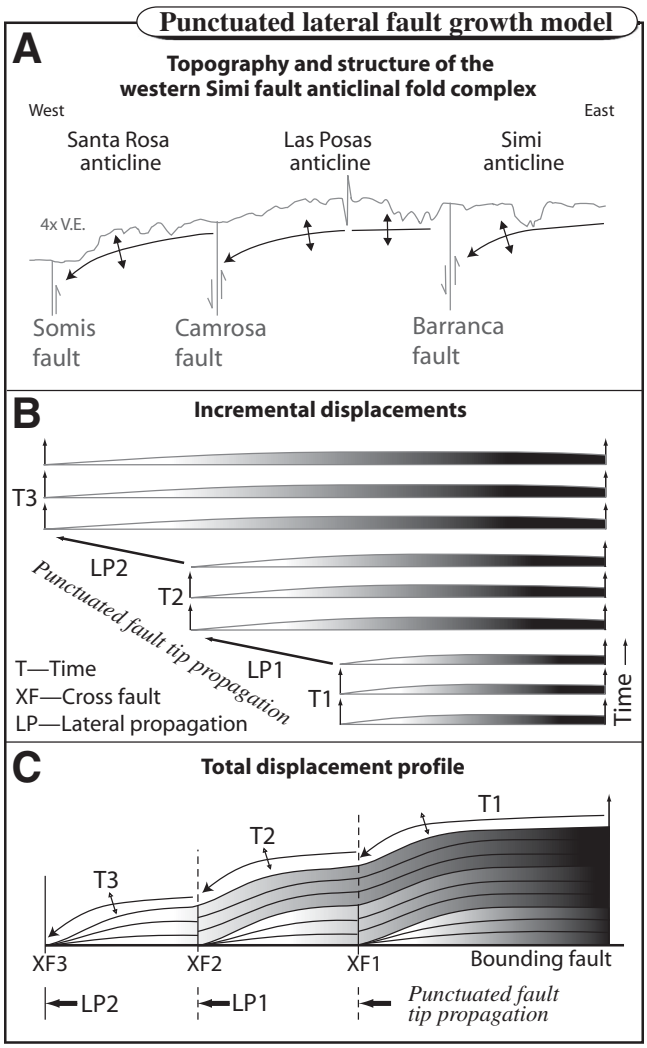

Figure 14. Punctuated lateral fault growth model for the Camarillo fold belt. The model incorporates properties of both the constant-length and increasing-length models (Fig. 13). (A) Topographic profile of the sutured Simi, Las Posas, and Santa Rosa anticlinal complex showing westward decrease in relief. V.E.—vertical exaggeration. (B) Incremental displacement profiles showing three time intervals (T1–T3), where fault displacement and fold amplification occur during constant-fault-length conditions that are punctuated by instances of westward lateral propagation (LP1 and LP2). (C) Total displacement profiles showing three linked west-plunging anticlines that lack east-plunging fold limbs, which results from incremental displacement profiles shown in C. Note that lateral fault growth during time intervals T1, T2, and T3 is constrained by the presence of an orthogonal cross-fault set (XF), such as those discussed in the text and shown in A.

able to rupture the Barranca fault and propagate into the Las Posas domain and join with the southern Simi fault (LP1, Fig. 14). We assume that because the southern Simi fault is a reactivated Miocene fault, and therefore an inherent crustal weakness, westward lateral propagation was rapid, and upon initial breaching of the Barranca fault, propagation may have extended all the way to the Camrosa fault. However, several ridge-parallel drainages along the crest of Las Posas anticlines (Fig. 4B) are suggestive of inherited drainage patterns typical of laterally propagating folds (i.e., Ramsey et al., 2008).

During time 2 (Fig. 14), incremental displacement of the Simi fault system resulted in continued amplification of the Simi anticline and the onset of folding in the Las Posas Hills. Because the locus of maximum uplift (dashed lines, Fig. 13) during this time was east of the Camarillo fold belt, hanging-wall folding in the Las Posas Hills was characterized by only west-plunging fold axes. In place of the east-plunging axis, north- and south-dipping Pleistocene strata of the Las Posas anticline are juxtaposed against the west-plunging Simi anticline (Fig. 4D). The Simi–Las Posas anticlines, now constrained on the west by the Camrosa fault during "time 2" (Fig. 14), amplified until threshold tectonic stresses were exceeded, and the Simi fault system was able to propagate into the Santa Rosa domain. The present system is illustrated by time 3 (Fig. 14), where three discrete west-plunging folds characterize the three structural domains. These folds are linked and are amplifying under constant-fault-length conditions, with the Somis fault limiting the westward growth of the current system (Fig. 14).

A fundamental question that arises from this model is whether the Simi fault system also grew eastward by the same mechanism. Geologic maps of the Simi Hills show the Simi fault and anticline abruptly terminating eastward near the northeastern corner of the Simi Valley (Fig. 2) (Kew, 1924; Hanson, 1980; Dibblee, 1992c). Although it might be expected that the Simi anticline near its eastern extent would plunge to the east, mapping shows no evidence of east-dipping strata, and the greatest structural relief occurs at the eastern terminus of the anticline. The Simi fault and fold end in a structurally complex zone of northwest-rending faults and folds in the footwall of the Santa Susana fault (Fig. 2), corresponding to the southward projection of the Gillibrand Canyon lateral ramp (Yeats, 1987). The ramp has been shown to influence Pliocene structures in the Santa Susana footwall and to the north in the east Ventura fold belt (Yeats, 1987), leading Yeats et al. (1994) to refer to the structure as a segment boundary. These observations suggest to us that growth of the Simi fault along its entire length has only been westward away from this structural segment boundary.

The Wheeler Ridge anticline is the only other well-studied fold that we know of that exhibits similar lateral propagation characteristics as those observed along the Simi fault. The Wheeler Ridge anticline, in the southern San Joaquin Valley of California, is characterized by a series of closely spaced (<2 km), shortening parallel faults that interrupt lateral propagation of the fold (i.e., Keller et al., 1989; Medwedeff, 1992; Mueller and Talling, 1997). Medwedeff (1992) interpreted the transverse faults as tear faults but indicated as much as 80 m of vertical displacement across the faults. Mueller and Talling (1997) concluded that, due to high strain gradients at the tip of a propagating fault, transverse tear faults should be common features, yet they knew of no other examples at the time of their study. Although there are many similarities in the kinematic evolution of the folds and faults in the Camarillo fold belt and deformation at Wheeler Ridge, the style of deformation in the Camarillo fold belt is largely controlled by the reactivation of older Miocene faults rather than being a consequence of differential shortening above a basal detachment, as interpreted at Wheeler Ridge (i.e., Medwedeff, 1992).

The presence of segmented east-striking reverse faults that are offset by north-striking transverse faults is discussed in numerous geologic investigations in Southern California (e.g., Wright, 1991; Shaw and Suppe, 1996; Davis et al., 1989; Dolan et al., 1995; Yeats et al., 1988). Given the polyphase deformational history of the Western Transverse Ranges, the structural inheritance and the style of contractional deformational observed in the Camarillo fold belt may be common in Southern California. The interpretation that faults grow by punctuated lateral fault growth has important implications for seismic hazard assessment, because it suggests that transverse faults are

capable of restricting the lateral growth of active faults and may be capable of limiting the maximum magnitude of seismic moment for a particular event. However, these faults appear to have a finite strength, and ultimately progressive displacement of the principal east-striking fault system results in lateral propagation across the preexisting tectonic barrier.

Seismic Hazard

Although beyond the scope of this paper, some of the results in this study are pertinent to the seismic hazard presented by the fault in the Camarillo fold belt, and, therefore, we provide preliminary estimates of several seismic hazard variables. The seismic hazard posed by a fault is a function of: (1) the size of the fault; (2) its rate of slip; (3) the recurrence interval; (4) time since last earthquake; (5) the degree to which a fault fails in conjunction with neighboring faults; and (6) the range of earthquake sizes generated by a fault. This study places constraints on the first two parameters, from which we use calculation methods of previous studies (i.e., Wells and Coppersmith, 1994; Dolan et al., 1995) to estimate the potential earthquake magnitudes and recurrence intervals for faults in the Camarillo fold belt. Moment magnitude estimates using regressions from global data sets from Wells and Coppersmith (1994) were calculated based on rupture length and modeled rupture area. However, because estimates of moment magnitude are empirically related to known geologic parameters and, therefore, affected by tectonic setting, we also utilized regression analysis of modeled fault plane area of Dolan et al. (1995). Regression analysis by Dolan et al. (1995) utilized Southern California earthquake events, and therefore, may better approximate potential earthquake magnitudes within the Camarillo fold belt than do global data sets.

To estimate potential earthquake magnitudes for faults based on rupture area, it is necessary to assume a potential seismic source depth, determine fault length, estimate the fault dip, and model the rupture area based on these parameters. Fault segment lengths are estimated based on geometric, geomorphic, and structural discontinuities that indicate lateral fault termination at segment boundaries. Rupture depth is based on historic earthquake rupture depths (>M_w 5.0) in the Western Transverse Ranges, which have typically occurred at depths from 8 km to 17 km (SCEC Earthquake Data Center, 2011). Rupture area is modeled based on 70° dipping fault planes that rupture upward from a depth of 8 km and 17 km along the entire length of the fault (Table 3).

Potential maximum moment magnitudes from the Camarillo fold belt are estimated to be within the range M_w 5.7 to M_w 6.8. with the southern Simi fault, characterizing the largest hazard for the region (Table 3). A somewhat lower moment magnitude of M_w 6.7 would be expected if the southern Simi and Santa Rosa faults are not kinematically linked across the Camrosa fault.

We use an average displacement of 1 m per seismic event based on paleoseismic investigations in the Camarillo fold belt (Gonzalez and Rockwell, 1991; Hitchcock et al., 1998) and slip rate estimates (Table 2) to calculate recurrence intervals (Table 3). Recurrence intervals along the main trend of the Simi fault zone are between 715 and 1100 yr (Table 3).

CONCLUSIONS

This study represents an integrated application of geochronology, paleoseismology, surface and subsurface geologic mapping, and structural analysis to estimate the timing, magnitude, and rates of deformation for perhaps the last unstudied fold belt in Southern California, the Camarillo fold belt. The fold belt is composed of no fewer than seven discrete west-plunging anticlinal folds that are developed in the hanging walls of east-striking north-dipping reverse fault segments that constitute the western extent of the Simi fault zone. The results presented here allow us to make the following conclusions and interpretations.

(1) The Camarillo fold belt is composed of discrete structural domains that are/were locally isolated from adjacent domains by an orthogonal north-striking fault set. Most Quaternary faults in the study area are reactivated Miocene transtensional faults that dip steeply (70°). The fold belt is characterized by rapid structural and geomorphic evolution, with all of the contractional deformation in the fold belt beginning after 125 ka, and some structures developing after ca. 25 ka. Hanging-wall deformation is characterized by anticlinal folding and fault-related uplift, where uplift due to folding is typically twice that of faulting. Fault slip rates are comparable (0.8–1.4 mm/yr) to other better-studied fold belts in Southern California, and, therefore, the Camarillo fold belt represents a significant seismic hazard to people living in Ventura and Los Angeles County. We estimate a potential maximum moment magnitude of M_w 6.8 along the main strand of the Simi fault; this is greater than the 1994 Northridge earthquake, which caused US$2 billion in damage and killed 57 people.

(2) Deformation in the Camarillo fold belt is locally controlled by the presence of north-striking cross faults, which limit the lateral growth of east-striking reverse faults. Parallel to strike of compound fold systems that have grown together to form a single topographic feature, the magnitudes of fault slip, folding, shortening, and structural relief decrease toward the west, with significant changes occurring at the locations of cross faults. In addition, the timing of deformation is,

TABLE 3. CAMARILLO FOLD BELT EARTHQUAKE MAGNITUDE MODEL AND FAULT RECURRENCE INTERVALS

Fault name	Structural domain	Length (km)*	Area (km²)†		Max (M_w)§		Max (M_w)#		Recurrence interval (yr)**
			Depth (5 km)	Depth (17 km)	Min	Max	Min	Max	
Simi fault system	Simi–Las Posas–Santa Rosa	31.4	267.3	401.0	6.5	6.7	6.6	6.8	715–1000
Southern Santa Rosa	Santa Rosa	4.4	37.5	79.6	5.7	6.0	5.9	6.2	900–1000
Santa Rosa Valley	Santa Rosa	4.8	40.9	86.8	5.8	6.1	5.9	6.2	770
No. Springville Fault	Northern Springville	6	51.1	108.5	5.9	6.2	6.0	6.3	715–910
So. Springville	Southern Springville	3.5	29.8	63.3	5.7	6.0	5.8	6.1	910–1100
Camarillo	–	5.5	46.8	99.5	5.8	6.1	6.0	6.3	590–910

Note: Gray box represents the compound Simi–Las Posas–Santa Rosa system discussed in text.
*Fault length is assumed to be the surface rupture length and may be slightly different than map length.
†Calculated fault area extends from 5 km and 17 km to the surface.
§Moment magnitude calculated from fault plane area with rupture at a depth of 12 km, using a regression of global reverse-motion earthquakes, $M_w = 4.33 + 0.90*\log(\text{area})$ from Wells and Coppersmith (1994).
#Moment magnitude calculated from fault plane area with rupture at a depth of 12 km, using a regression of global reverse-motion earthquakes, $M_w = 4.56 + 0.86*\log(\text{area})$ from Dolan et al. (1995).
**Average coseismic slip was assumed to be 1 m based on previous paleoseismic observations from the Springville and Simi faults (Gonzalez and Rockwell, 1991; Hitchcock et al., 1998). Recurrence interval was calculated by dividing average slip by the rate of fault slip (Table 3).

locally, younger toward the west. We interpret these observations to indicate that the Simi fault is growing westward by a process herein referred to as punctuated lateral propagation. Our model suggests that westward lateral fault growth occurs in discrete pulses that are separated by intervals of fault displacement and fold amplification during constant-fault-length conditions.

ACKNOWLEDGMENTS

The initial field work and analytical costs were funded by the Southern California Earthquake Center (SCEC award 120044), a consortium of earthquake scientists funded by the National Science Foundation and the U.S. Geological Survey National Earthquake Hazard Reduction Program (NEHRP award 8HQGR0073). Additional support was provided by the University of California, Santa Barbara, in the form of teaching assistantships to support DeVecchio during his dissertation research. We owe special thanks to GeoSoils, Inc., and Earth Systems Southern California for letting us access paleoseismic trenches, and John Brennon, who funded reopening trenches on his property on the Camarillo anticline. Sincere thanks go to James R. Budahn for determining radioisotope concentrations using instrumental neutron activation analysis (INAA). We thank Robert Yeats, Mike Oskin, Shannon Mehan, Tim Little, and anonymous reviewers for constructive reviews of early drafts of this manuscript.

REFERENCES CITED

Aitken, M.J., 1985, Thermoluminescence dating: Oxford, Academic Press, 276 p.

Aitken, M.J., 1998, An Introduction to Optical Dating: The Dating of Quaternary Sediments by the Use of Photon-Stimulated Luminescence: Oxford, UK, Oxford University Press, 267 p.

Bailey, T.L., 1951, Geology of a portion of Ventura basin: Los Angeles and Ventura Counties, California, scale 1:48,000.

Blake, T.F., 1991a, Synopsis of the character and recency of faulting along the Simi–Santa Rosa fault system, *in* Blake, T.F., ed., Engineering Geology along the Simi–Santa Rosa Fault System and Adjacent Areas, Simi Valley to Camarillo Ventura County, California: Southern California Section Association of Engineering Geologists, Annual Field Trip Guidebook, v. 1, p. 96–118.

Blake, T.F., ed., 1991b, Engineering Geology along the Simi–Santa Rosa Fault System and Adjacent Areas, Simi Valley to Camarillo Ventura County, California: Annual Field Trip Guidebook Volume 2: Southern California Section Association of Engineering Geologists, 383 p.

Boales, P.V., 1991, Near-surface geology of the southwestern Las Posas Hills area, Camarillo, Ventura County, California, *in* Blake, T.F., ed., Engineering Geology along the Simi–Santa Rosa Fault System and Adjacent Areas, Simi Valley to Camarillo Ventura, California: Southern California Section Association of Engineering Geologists, Annual Field Trip Guidebook, v. 2, p. 230–243.

Childs, C., Nicol, A., Walsh, J.J., and Watterson, J., 2003, The growth and propagation of synsedimentary faults: Journal of Structural Geology, v. 25, no. 4, p. 633–648, doi:10.1016/S0191-8141(02)00054-8.

Crowell, J.C., 1976, Implications of crustal stretching and shortening of coastal Ventura Basin, California, *in* Aspects of the Geological History of the California Continental Borderland: American Association of Petroleum Geologists, Pacific Section, Miscellaneous Publication 24, p. 365–382.

Dahlen, M.Z., 1992, Sequence stratigraphy, depositional history, and middle to late Quaternary sea levels of the Ventura Shelf, California: Quaternary Research, v. 38, no. 2, p. 234–245, doi:10.1016/0033-5894(92)90059-R.

Davis, T.L., Namson, J., Yerkes, R.F., and Anonymous, 1989, A cross section of the Los Angeles area: Seismically active fold and thrust belt, the 1987 Whittier Narrows earthquake, and earthquake hazard: Journal of Geophysical Research, v. 94, no. B7, p. 9644–9664.

DeVecchio, D.E., Heermance, R.V., Fuchs, M., and Owen, L.A., 2012, Climate-controlled landscape evolution in the Western Transverse Ranges, California: Insights from Quaternary geochronology of the Saugus Formation and strath terrace flights: Lithosphere, v. 4, doi: 10.1130/L176.1.

Dibblee, T.W., 1990, Geologic Map of the Camarillo and Newbury Park Quadrangles, Ventura County: Dibblee Geological Foundation Santa Barbara, California, scale 1:24,000, 1 sheet.

Dibblee, T.W., 1992a, Geologic Map of the Moorpark Quadrangle, Ventura County: Dibblee Geological Foundation, Santa Barbara, California, scale 1:24,000, 1 sheet.

Dibblee, T.W., 1992b, Geologic Map of the Simi Quadrangle, Ventura County: Dibblee Geological Foundation, Santa Barbara, California, scale 1:24,000, 1 sheet.

Dibblee, T.W., Jr., 1992c, Geologic map of the Santa Susana quadrangle, Ventura County, California: Division of Mines and Geology and Geological Survey (U.S.), and Dibblee Geological Foundation, scale 1:24,000, 1 sheet.

Dolan, J.F., Sieh, K., Rockwell, T.K., Yeats, R.S., Shaw, J., Suppe, J., Huftile, G.J., and Gath, E.M., 1995, Prospects for larger or more frequent earthquakes in the Los Angeles metropolitan region: Science, v. 267, no. 5195, p. 199–205, doi:10.1126/science.267.5195.199.

Dolan, J.F., Sieh, K., and Rockwell, T.K., 2000, Late Quaternary activity and seismic potential of the Santa Monica fault system, Los Angeles, California: Geological Society of America Bulletin, v. 112, no. 10, p. 1559–1581, doi:10.1130/0016-7606(2000)112<1559:LQAASP>2.0.CO;2.

Dolan, J.F., Christofferson, S.A., and Shaw, J.H., 2003, Recognition of paleoearthquakes on the Puente Hills blind thrust fault, California: Science, v. 300, no. 5616, p. 115–118, doi:10.1126/science.1080593.

Donnellan, A., Hager, B.H., and King, R.W., 1993, Discrepancy between geological and geodetic deformation rates in the Ventura Basin: Nature, v. 366, no. 6453, p. 333–336, doi:10.1038/366333a0.

Durrell, C., 1954, Geology of the Santa Monica Mountains, Los Angeles and Ventura Counties, California: Map sheet 8, *in* Jahns, R., ed., Geology of Southern California: California Division of Mines Bulletin 170.

Earth Systems Southern California, 2005, Fault Rupture Hazard Investigation, 7.81-Acre Parcel, Proposed Mobile Home Park Expansion, Camarillo, California: Earth Systems Southern California Report 05-3-23, File No. VT-23220-01, 117 p.

Ehrenspeck, H.E., 1972, Geology and Miocene Volcanism of the Eastern Conejo Hills Area, Ventura County, California [M.A. thesis]: Santa Barbara, California, University of California Santa Barbara, vii, 135 leaves, bound.

Fuchs, M., and Lang, A., 2001, OSL dating of coarse-grain fluvial quartz using single-aliquot protocols on sediments from NE Peloponnese, Greece, *in* Gruen, R., and Wintle, A.G., eds., Quaternary Science Reviews: Oxford, Pergamon, p. 783–787.

Fuchs, M., and Wagner, G.A., 2003, Optical dating of sediments: Recognition of insufficient bleaching by small aliquots of quartz for reconstructing soil erosion in Greece: Quaternary Science Reviews, v. 22, p. 1161–1167, doi:10.1016/S0277-3791(03)00039-8.

Fuchs, M., Woda, C., and Buerkert, A., 2007, Chronostratigraphy of a sediment record from the Hajar Mountain range in north Oman: Implications for optical dating of insufficiently bleached sediments, *in* Grun, R., and Roberts, R.G., eds., Quaternary Geochronology: Amsterdam, Netherlands, Elsevier, p. 202–207.

Geosoils, Inc., 2006, Preliminary Geotechnical Investigation APN 162-0-200-015, Tentative Tract 5724 South of the Intersection of Sevilla St. and Barcelona Ave, Camarillo, Ventura County, California: Geosoils, Inc.

Glenn, D., 1991, A fault trenching study along the Springville fault zone, Camarillo, California, *in* Blake, T.F., ed., Engineering Geology along the Simi–Santa Rosa Fault System and Adjacent Areas, Simi Valley to Camarillo Ventura, California: Southern California Section Association of Engineering Geologists, Annual Field Trip Guidebook, v. 2, p. 205–208.

Gonzalez, T., and Rockwell, T.K., 1991, Holocene activity of the Springville fault in Camarillo, Transverse Ranges, Southern California; preliminary observations, *in* Blake T.F., ed., Engineering Geology along the Simi–Santa Rosa Fault System and Adjacent Areas, Simi Valley to Camarillo Ventura, California: Southern California Section Association of Engineering Geologists, Annual Field Trip Guidebook, v. 2, p. 369–383.

Hanson, D.W., 1980, Surface and Subsurface Geology of the Simi Valley Area, Ventura County, California [Master's thesis]: Corvallis, Oregon, Oregon State University, 112 p.

Hanson, R.T., Martin, P., and Koczot, K.M., 2003, Simulation of Ground-Water/Surface-Water Flow in the Santa Clara–Calleguas Ground-Water Basin, Ventura County, California: U.S. Geological Survey Water Resources Report, 157 p.

Hitchcock, C.S., Treiman, J.A., Lettis, W.R., Simpson, G.D., and Anonymous, 1998, Paleoseismic investigation of the Simi fault at Arroyo Simi, Simi Valley, Ventura County, California: Geological Society of America Abstracts with Programs, v. 30, no. 5, p. 19–20.

Huftile, G.J., and Yeats, R.S., 1995, Convergence rates across a displacement transfer zone in the Western Transverse Ranges, Ventura Basin, California: Journal of Geophysical Research, ser. B, Solid Earth and Planets, v. 100, no. 2, p. 2043–2067, doi:10.1029/94JB02473.

Ingersoll, R.V., 2001, Tectonostratigraphy of the Santa Monica Mountains, southern California, *in* Wright, T.L., and Yeats, R.S., eds., Geology and Tectonics of the San Fernando Valley and East Ventura Basin, California: Los Angeles, California, Pacific Section, American Association of Petroleum Geologists, Guidebook GB 77, p. 63–70.

Jackson, J., Norris, R., Youngson, J., and Wojtal, S.F., 1996, The structural evolution of active fault and fold systems in central Otago, New Zealand: Evidence revealed by drainage patterns: Journal of Structural Geology, v. 18, no. 2–3, p. 217–234, doi:10.1016/S0191-8141(96)80046-0.

Jakes, M.C., 1979, Surface and Subsurface Geology of the Camarillo and Las Posas Hills Area, Ventura County, California [Master's thesis]: Corvallis, Oregon, Oregon State University 117 p.

Kamerling, M.J., and Luyendyk, B.P., 1979, Tectonic rotations of the Santa Monica Mountains region, Western Transverse Ranges, California, suggested by paleomagnetic vectors: Geological Society of America Bulletin, v. 90, no. 4, Part 1, p. 331– 337.

Keller, E.A., and DeVecchio, D.E., 2012, Tectonic geomorphology of active folding and development of transverse drainages, *in* Shroder, J., Jr., and Owen, L.A.P., eds., Local Scale Tectonic Geomorphology: Amsterdam, Elsevier, Treatise on Geomorphology, v. 5, no. 13 (in press).

Keller, E.A., and Gurrola, L.D., 2000, Earthquake Hazard of the Santa Barbara Fold Belt, final report to the U.S. Geological Survey: National Earthquake Reduction Program (NEHRP), Award #527726, 106 p.

Keller, E.A., and Pinter, N., 2002, Active Tectonics, 2nd ed: Upper Saddle Rivers, Prentice Hall, 363 p.

Keller, E.A., Zepeda, R.L., Rockwell, T.K., Ku, T.L., and Dinklage, W.S., 1998, Active tectonics at Wheeler Ridge, southern San Joaquin Valley, California: Geological Society of America Bulletin, v. 110, no. 3, p. 298–310.

Kew, W.S.W., 1924, Geology and oil resources of a part of Los Angeles and Ventura Counties, California: U.S. Geological Survey Bulletin 753, 202 p.

Kile, M.B., McMillan, K., McNamara, J.E., Primas, T.M., and Butler, G., 1991, Structural geology of the westernmost Camarillo Hills, Ventura County, California, *in* Blake, T.F., ed., Engineering Geology along the Simi–Santa Rosa Fault System and Adjacent Areas, Simi Valley to Camarillo Ventura, California: Southern California Section Association of Engineering Geologists, Annual Field Trip Guidebook, v. 1, p. 67–75.

Lajoie, K.R., Sarna-Wojcicki, A.M., Yerkes, R.F., and Cooper, J.D., 1982, Quaternary chronology and rates of crustal deformation in the Ventura area, California, *in* Cooper, J.D., ed., Neotectonics in Southern California: Geological Society of America Cordilleran Section, Field Trip Guidebook, p. 43–51.

Larsen, S.C., Agnew, D.C., and Hager, B.H., 1993, Strain accumulation in the Santa-Barbara channel—1970–1988: Journal of Geophysical Research, Solid Earth, v. 98, no. B2, p. 2119–2133, doi:10.1029/92JB02043.

Levi, S., and Yeats, R.S., 1993, Paleomagnetic constraints on the initiation of uplift on the Santa Susana fault, Western Transverse Ranges, California: Tectonics, v. 12, no. 3, p. 688–702, doi:10.1029/93TC00133.

Luyendyk, B.P., Kamerling, M.J., and Terres, R., 1980, Geometric model for Neogene crustal rotations in southern California: Geological Society of America Bulletin, v. 91, no. 4, p. I 211-I 217.

McNamara, J.E., McMillan, K., Lopez, W.B., Kile, M.B., Butler, G., and Van Alstine, D., 1991, Saugus Formation stratigraphy, Camarillo Hills, Ventura County, California, *in* Blake, T.F., ed., Engineering Geology along the Simi–Santa Rosa Fault System and Adjacent Areas, Simi Valley to Camarillo Ventura, California: Southern California Section Association of Engineering Geologists, Annual Field Trip Guidebook, v. 1, p. 57–66.

Medwedeff, D., 1992, Geometry and kinematics of an active, laterally propagating wedge thrust, Wheeler Ridge, California, *in* Mitra, S., Fisher, G.W., Phillips, O.M., Stanley, S.M., and Strobel, D.F., eds., Structural geology of fold and thrust belts: Baltimore, Johns Hopkins University Press, p. 3–28.

Mueller, K., and Talling, P., 1997, Geomorphic evidence for tear faults accommodating lateral propagation of an active fault-bend fold, Wheeler Ridge, California: Journal of Structural Geology, v. 19, no. 3–4, p. 397–411.

Murray, A.S., and Olley, J.M., 2002, Precision and accuracy in the optically stimulated luminescence dating of sedimentary quartz: A status review: Journal on Methods and Applications of Absolute Chronology: Geochronometria, v. 21, p. 1–16.

Murray, A.S., and Wintle, A.G., 2000, Luminescence dating of quartz using an improved single-aliquot regenerative-dose protocol: Radiation Measurements, v. 32, no. 1, p. 57–73, doi:10.1016/S1350-4487(99)00253-X.

Murray, A.S., Olley, J.M., and Caitcheon, G.G., 1995, Measurement of equivalent doses in quartz from contemporary water-lain sediments using optically stimulated luminescence: Quaternary Science Reviews, v. 14, no. 4, p. 365–371, doi:10.1016/0277-3791(95)00030-5.

Namson, J.S., and Davis, T.L., 1988, Seismically active fold and thrust belt in the San Joaquin Valley, central California: Geological Society of America Bulletin, v. 100, no. 2, p. 257–273, doi:10.1130/0016-7606(1988)100<0257:SAFATB>2.3.CO;2.

Namson, J., and Davis, T.L., 1991, Cross section of the western Santa Monica Mountains to the San Andreas fault, *in* Blake, T.F., ed., Engineering Geology along the Simi–Santa Rosa Fault System and Adjacent Areas, Simi Valley to Camarillo Ventura, California: Southern California Section Association of Engineering Geologists, Annual Field Trip Guidebook, v. 1, p. 87–95.

Nicholson, C., Sorlien, C.C., Atwater, T., Crowell, J.C., and Luyendyk, B.P., 1994, Microplate capture, rotation of the Western Transverse Ranges, and initiation of the San Andreas transform as a low-angle fault system: Geology, v. 22, no. 6, p. 491–495, doi:10.1130/0091-7613(1994)022<0491:MCROTW>2.3.CO;2.

Nicol, A., Walsh, J., Berryman, K., and Nodder, S.D., 2005, Growth of a normal fault by the accumulation of slip over millions of years: Journal of Structural Geology, v. 27, no. 2, p. 327–342, doi:10.1016/j.jsg.2004.09.002.

Oskin, M., Sieh, K., Rockwell, T., Miller, G., Guptill, P., Curtis, M., McArdle, S., and Elliot, P., 2000, Active parasitic folds on the Elysian Park anticline: Implications for seismic hazard in central Los Angeles, California: Geological Society of America Bulletin, v. 112, no. 5, p. 693–707, doi:10.1130/0016-7606(2000)112<693:APFOTE>2.0.CO;2.

Pasta, D., 1958 Geology of the Las Posas–Camarillo Hills Area, Ventura County, California [Master's thesis]: Los Angeles, California, University of California, 59 p.

Pressler, E., 1929, The Fernando Group in the Las Posas-South Mountain District, Ventura County, California: University of California Publications, Bulletin of the Department of Geological Sciences, v. 18, no. 13, p. 325-345.

Prinz, H., 1982, Abriss der Ingenieurgeologie; Mit Grundlagen der Boden- und Felsmechanik sowie des Erd-, Grund- und Tunnelbaus: Engineering geology; soil and rock mechanics; surface, underground and tunnel construction: Stuttgart, Federal Republic of Germany (DEU), Ferdinand Enke, 419 p.

Ramsey, L.A., Walker, R.T., and Jackson, J., 2008, Fold evolution and drainage development in the Zagros Mountains of Fars Province, SE Iran: Basin Research, v. 20, no. 1, p. 23–48, doi:10.1111/j.1365-2117.2007.00342.x.

Rockwell, T.K., Keller, E.A., Clark, M.N., and Johnson, D.L., 1984, Chronology and rates of faulting of Ventura River terraces, California: Geological Society of America Bulletin, v. 95, no. 12, p. 1466–1474, doi:10.1130/0016-7606(1984)95<1466:CAROFO>2.0.CO;2.

Ruff, R., and Shlemon, R.J., 1991, Character and recency of faulting along a portion of the northern Springville fault, Camarillo, Ventura County, California, *in* Blake, T.F., ed., Engineering Geology along the Simi–Santa Rosa Fault System and Adjacent Areas, Simi Valley to Camarillo Ventura, California: Southern California Section Association of Engineering Geologists, Annual Field Trip Guidebook, v. 1, p. 147–165

Scheffer, F., and Schachtschabel, P., 1998, Lehrbuch der Bodenkunde: Stuttgart, Germany, Enke Verlag, 442 p.

Scientists of the U.S. Geological Survey and Southern California Earthquake Center, 1994, The magnitude 6.7 Northridge, California, earthquake of 17 January, 1994: Science, v. 266, p. 389–397, doi:10.1126/science.266.5184.389.

Shaw, J.H., and Suppe, J., 1996, Earthquake hazards of active blind-thrust faults under the central Los Angeles Basin, California: Journal of Geophysical Research, ser. B, Solid Earth and Planets, v. 101, no. 4, p. 8623–8642, doi:10.1029/95JB03453.

Shaw, J.H., Plesch, A., Dolan, J.F., Pratt, T.L., and Fiore, P., 2002, Puente Hills blind-thrust system, Los Angeles, California: Bulletin of the Seismological Society of America, v. 92, no. 8, p. 2946–2960, doi:10.1785/0120010291.

Shen, Z.-K., Agnew, C.D., and King, R.W., 2003, The SCEC Crustal Motion Map, Version 3.0: Los Angeles, Southern California Earthquake Center (available at (http://epicenter.usc.edu/cmm3/).

Southern California Earthquake Center (SCEC) Earthquake Data Center, 2011, Earthquake Catalog, 221 p.: http://www.data.scec.org/eq-catalogs/date_mag_loc.php (last accessed 11 October 2011).

Treiman, J.A., 1997, Springville, Camarillo and Related Faults in the Camarillo and Santa Paula Quadrangles, Ventura County: California Division of Mines and Geology Fault Evaluation Report FER-237, 21 p.

Treiman, J.A., 1998, Simi–Santa Rosa Fault Zone in the Moorpark, Newbury Park, Simi Valley East, Simi Valley West, Thousand Oaks Quadrangles, Ventura County: California Division of Mines and Geology Fault Evaluation Report FER-244, 35 p.

Wallinga, J., 2002, On the detection of OSL age overestimations using single-aliquot techniques: Geochronometria, v. 21, p. 17–26.

Weber, F.H., Kiessling, E.W., Sprotte, E.C., Johnson, J.A., Sherburne, R.W., and Cleveland, G.B., 1976, Seismic Hazards Study of Ventura County: California Department of Conservation California Division of Mines and Geology Open-File Report 76-5, 396 p.

Weigand, P.W., Savage, K.L., and Nicholson, C., 2002, The Conejo Volcanics and other Miocene volcanic suites in southwestern California, *in* Barth, A., ed., Contributions to Crustal Evolution of the Southwestern United States: Geological Society of America Special Paper 365, p. 187–204.

Wells, D.L., and Coppersmith, K.J., 1994, New empirical relationships among magnitude, rupture length, rupture width, rupture area, and surface displacement: Bulletin of the Seismological Society of America, v. 84, no. 4, p. 974–1002.

Whitney, R.A., and Gath, E.M., 1991, Structure, tectonics, and surface rupture hazard at the Las Posas anticline, Ventura County, California, *in* Blake, T.F., ed., Engineering Geology along the Simi–Santa Rosa Fault System and Adjacent Areas, Simi Valley to Camarillo Ventura, California: Southern California Section Association of Engineering Geologists, Annual Field Trip Guidebook, v. 2, p. 164–182.

Williams, R.E., 1983, Miocene volcanism in the central Conejo Hills and western Simi Valley, Ventura, California, *in* Squires, R.L., and Folewicz, M.V., eds., Cenozoic Geology of the Simi Valley Area, Southern California: Los Angeles, California, Society of Economic Paleontologists and Mineralogists, Pacific Section, p. 183–190.

Winterer, E.L., and Durham, D.L., 1958, Geologic map of a part of the Ventura Basin, Los Angeles County, California: U.S. Geological Survey, scale 1:24,000.

Wright, T.L., 1991, Structural geology and tectonic evolution of the Los Angeles basin, California, *in* Biddle, K.T., ed., Active Margins Basins: American Association of Petroleum Geologist Memoir 52, p. 35–135.

Working Group on California Earthquake Probabilities (WGCEP), 1995, Seismic hazards in southern California: Probable earthquakes, 1994–2024: Seismological Society of America Bulletin, v. 85, p. 379–439.

Working Group on California Earthquake Probabilities (WGCEP), 2007, The Uniform California Earthquake Rupture Forecast, Version 2 (UCERF 2): U.S. Geological Survey Open-File Report 2007-1437, 96 p.

Yeats, R.S., 1965, Pliocene seaknoll at South Mountain, Ventura Basin, California: Bulletin of the American Association of Petroleum Geologists, v. 49, no. 5, p. 526–546.

Yeats, R.S., 1977, High rates of vertical crustal movement near Ventura, California: Science, v. 196, no. 4287, p. 295–298, doi:10.1126/science.196.4287.295.

Yeats, R.S., 1981, Quaternary flake tectonics of the California Transverse Ranges: Geology, v. 9, no. 1, p. 16–20.

Yeats, R.S., 1983, Large-scale Quaternary detachments in Ventura Basin, Southern California: Journal of Geophysical Research, v. 88, no. B1, p. 569–583.

Yeats, R.S., 1987, Late Cenozoic structure of the Santa Susana fault zone: U.S. Geological Survey Professional Paper 1339, p. 137–160, colored map, scale 1:48,000.

Yeats, R.S., 1988a, Late Quaternary slip rate on the Oak Ridge fault, Transverse-Ranges, California—Implications for seismic risk: Journal of Geophysical Research, ser. B, Solid Earth and Planets, v. 93, no. B10, p. 12,137–12,149, doi:10.1029/JB093iB10p12137.

Yeats, R.S., 1988b, Oak Ridge Fault, Ventura Basin, California; Slip Rates and Late Quaternary History: U.S. Geological Survey Final Report Grant 14-08-0001-G1194, 32 p.

Yeats, R.S., Huftile, H.J., and Grigsby, F.B., 1988, Oak Ridge Fault, Ventura fold belt, and the Sisar décollement, Ventura Basin: California Geology, v. 16, p. 1112–1116.

Yeats, R.S., Huftile, G.J., and Stitt, L.T., 1994, Late Cenozoic tectonics of the East Ventura Basin, Transverse Ranges, California: American Association of Petroleum Geologists Bulletin, v. 78, no. 7, p. 1040–1074.

Yeats, R.S., Sieh, K., and Allen, C.R., 1997, The Geology of Earthquakes: Oxford, UK, Oxford University Press, p. 362.

Yerkes, R.F., Sarna-Wojcicki, A.M., and Lajoie, K.R., 1987, Geology and Quaternary Deformation of the Ventura Area: U.S. Geological Survey Professional Paper P1339, p. 169–178.

MANUSCRIPT RECEIVED 29 JANUARY 2011
REVISED MANUSCRIPT RECEIVED 31 OCTOBER 2011
MANUSCRIPT ACCEPTED 3 NOVEMBER 2011

Printed in the USA